REVIEW

JAAS
www.rsc.org/jaas

Comparing several atomic spectrometric methods to the super stars: special emphasis on laser induced breakdown spectrometry, LIBS, a future super star†

James D. Winefordner, Igor B. Gornushkin, Tiffany Correll, Emily Gibb, Benjamin W. Smith and Nicoló Omenetto

Department of Chemistry, University of Florida, Gainesville FL 32611, USA

Received 9th January 2004, Accepted 22nd March 2004
First published as an Advance Article on the web 18th May 2004

The "super stars" of analytical atomic spectrometry are electrothermal atomization-atomic absorption spectrometry (ETA-AAS), inductively coupled plasma-atomic emission spectrometry (ICP-AES) and inductively coupled plasma-mass spectrometry (ICP-MS). Many other atomic spectrometric methods have been used to determine levels of elements present in solid, liquid and gaseous samples, but in most cases these other methods are inferior to the big three super star methods. The other atomic methods include glow discharge emission, absorption and mass spectrometric methods, laser excited fluorescence emission and ionization methods, and flame and microwave plasma emission and mass spectrometric methods. These "lesser" methods will be compared to the "super star" methods based on a number of figures of merit, including detection power, selectivity, multi-element capability, cost, applications, and "age" of the methods. The "age" of the method will be determined by a modification of the well-known Laitinen "Seven Ages of an Analytical Method" (H.A. Laitinen, *Anal. Chem.*, 1973, **45**, 2305). Calculations will show that certain methods are capable of single atom detection, including several atomic absorption methods, as well as laser atomic ionization and fluorescence methods. The comparison of methods will indicate why the "super stars" of atomic spectrometric methods will continue to retain their status and what must be done for the lesser atomic methods to approach "super star" status. Certainly most of the lesser atomic spectrometric methods will have a limited place in the analytical arena. Because of the wide current interest and research activity, special emphasis will be placed on the technique of laser induced breakdown spectrometry (LIBS). Its current status and future developments will therefore be reviewed.

Comparison of methods

Introduction

Atomic spectroscopy is the most common approach to elemental analysis. The three major atomic spectroscopic methods (the "super stars") are electrothermal atomization-atomic absorption spectrometry, ETA-AAS, inductively coupled plasma-atomic emission spectrometry, ICP-AES, and inductively coupled plasma-mass spectroscopy, ICP-MS. These methods have been the predominant methods used for elemental analysis of samples of importance in industrial, biological, environmental, pharmaceutical, and forensic science. In this paper, we will compare a number of more specialized atomic spectroscopic methods to the three major methods. The more specialized methods to be compared are:

(i) atomic emission methods using flames, arcs, sparks, microwave plasmas, glow discharges, laser induced plasmas, furnace plasmas;

(ii) atomic absorption methods using flames, furnaces, and glow discharges with line or continuum sources and with or without wavelength or frequency modulation;

(iii) other atomic absorption methods using flames or other atom cells with cavity ringdown, multipass absorption, and intracavity absorption and coherent forward scatter;

(iv) photoacoustic detection;

(v) atomic fluorescence methods using flames, furnaces, glow discharges, cold vapor cells and ICPs with excitation by conventional line and continuum sources as well as laser excitation; and

(vi) atomic ionization methods using flames or furnaces and laser excitation.

The general principles of each method will be given. Each spectroscopic method will be evaluated with respect to a number of figures of merit including detection power, selectivity, linear dynamic range, capability for single atom detection (SAD) and single atom measurement (SAM), capability for absolute analysis, where analysis is performed without calibration standards, multi-element capability, the extent of research and application activity, and the age of the method. The age will be a modification of the original Laitinen[1] "Seven Ages of an Analytical Method" and further modification of those described by Fassel[2] and Hieftje.[3,4]

Certainly, atomic emission spectroscopy with the flame, the dc arc and the ac spark was among the first techniques to be used for qualitative and quantitative analysis. The dc arc and ac spark are still two of the widely used methods, although the source of excitation has shifted from the arc and spark to the ICP as well as some lesser used sources. Even so, a survey taken by *Spectroscopy* magazine shows the current demand for arc and spark atomic emission spectrometry is still high (10%) compared to 16% for ICP-AES, 10% for ICP-MS, and 21% for atomic absorption spectroscopy.[5]

This paper is a combination of a tutorial description of the methods as well as our opinion on the status of each method compared to the 3 major atomic spectroscopic methods. In addition, we will highlight LIBS, laser induced breakdown spectroscopy, because of its current interest (over 1500 papers in the past 5 years). The authors do not intend to be comprehensive in listing references but rather will select ones which give tutorial and/or novel discussions, theories, and uses.

The processes

In Fig. 1, the transitions responsible for most atomic spectrometric methods are shown (AAS, atomic absorption spectrometry, AES, atomic emission spectrometry, AFS, atomic

† Presented at the 2004 Winter Conference on Plasma Spectrochemistry, Fort Lauderdale, FL, USA, January 5–10, 2004, and as a plenary lecture at the 2003 CSI, Granada, Spain.

DOI: 10.1039/b400355c

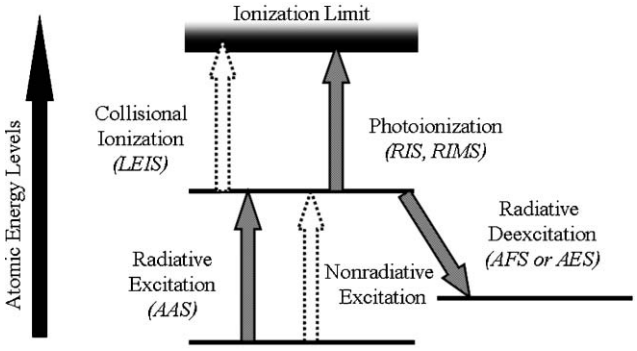

Fig. 1 Representation of processes in atomic spectroscopic methods.

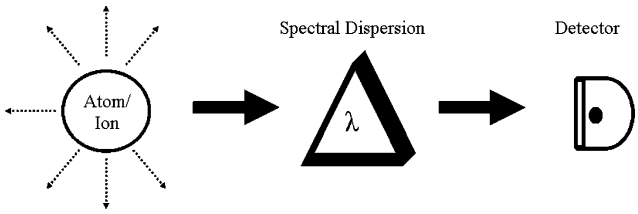

Sources of Excitation:

1. Flame
2. Inductively Coupled Plasma (ICP)
3. Glow Discharge (GD)
4. Laser Spark (LIBS)
5. Furnace
6. Microwave Plasma
7. DC Arc
8. AC Spark

Fig. 2 Schematic representation of atomic emission spectroscopy (AES) with types of sources.

fluorescence spectrometry, LEIS, laser enhanced ionization spectrometry, RIS, resonance ionization spectrometry, and RIMS, resonance ionization mass spectrometry). It should be noted that AAS includes all of the intracavity absorption

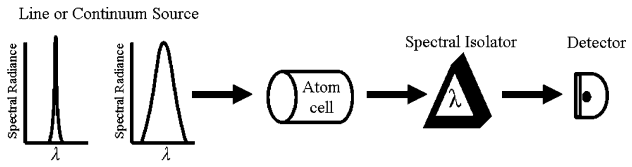

Sources:

1. Hollow Cathode Lamp (HCL)
2. Electrodeless Discharge Lamp (EDL)
3. Diode Laser
4. Xenon Arc Lamp

Methods of Atomization:

1. Flame
2. Furnace
3. Glow Discharge
4. Cold Vapor

Fig. 3 Schematic representation of atomic absorption spectroscopy (AAS) with types of sources and atomizers.

methods, cavity ringdown spectrometry, CRS, and coherent forward scatter, CFS, also known as atomic magneto-optic rotation spectrometry, AMORS, as well as wavelength and frequency modulation atomic absorption methods. All of the atomic absorption techniques based on cavities were described schematically and theoretically, including signal-to-noise expressions, in a previous article by Winefordner, *et al.*[6]

General principles of individual methods

The general principles of the various spectroscopic methods to be compared are given in Fig. 2 (atomic emission spectroscopic methods, AES),[7–10] Fig. 3 (atomic absorption spectroscopic methods, AAS),[11,12] Fig. 4 (cavity ringdown spectroscopy, CRS),[13] Fig. 5 (coherent forward scatter, CFS),[14] Fig. 6 (photoacoustic detection),[15] Fig. 7 (optogalvanic/photoacoustic spectroscopy),[16] Fig. 8 (atomic fluorescence spectroscopic methods, AFS),[17,18] Fig. 9 (laser enhanced ionization spectroscopy, LEIS),[19–21] Fig. 10 (resonance ionization spectroscopy, RIS),[19–26] Fig. 11 (resonance ionization mass spectrometry, RIMS),[22–24] Fig. 12 (inductively coupled plasma mass spectrometry, ICP-MS).[7,8] Detailed discussions of each spectroscopic method are given in many texts and specialized books and

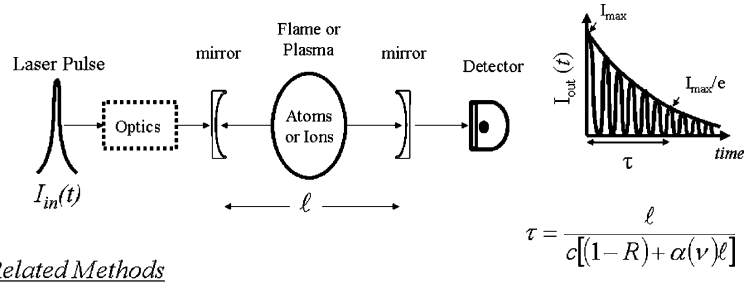

Related Methods

1. Multipass Absorption Spectroscopy (MPAS)
2. Cavity Enhanced Absorption Spectroscopy (CEAS)
3. Intracavity Absorption Spectroscopy (ICAS)
4. Frequency Modulated Optical Heterodyne Spectroscopy (NICE-OHMS)

Fig. 4 Schematic representation of cavity ringdown atomic spectroscopy with several related cavity methods.

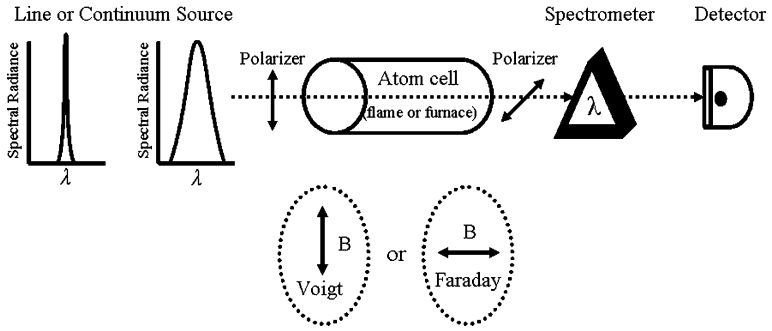

Fig. 5 Schematic representation of coherent forward scatter atomic spectroscopy (coherent forward scatter spectrometry, CFS, or atomic magneto-optic rotation spectrometry, AMORS).

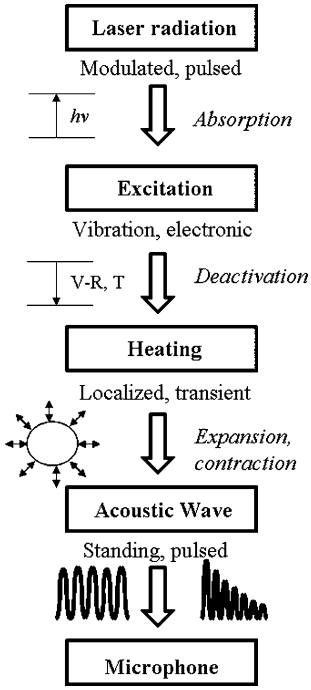

Fig. 6 Representation of processes occurring in photoacoustic detection.

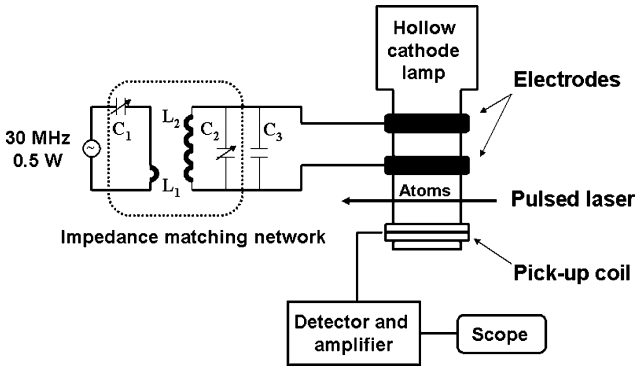

Fig. 7 Schematic representation of optogalvanic/photoacoustic detection of atoms and ions in a hollow cathode lamp.

review articles and chapters and will not be given here except for several references which can be referred to for more details.

Figures of merit of the methods

In Table 1, the figures of merit (FOM) considered for comparison of the atomic spectroscopic methods are listed. All of the figures of merit will be denoted by values of 5, 4, 3, 2, 1, where 5 is highest (excellent) and 1 is lowest (poor). Several of the FOM's need further discussion.[27–32]

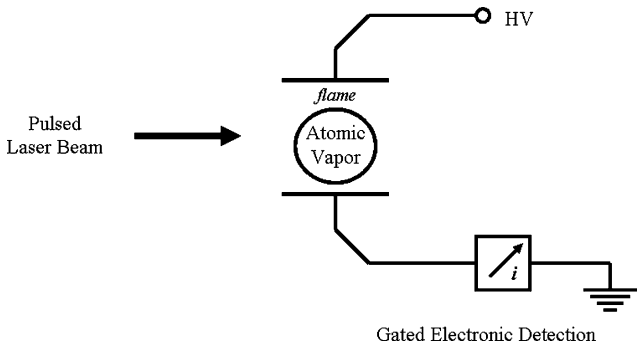

Fig. 9 Schematic representation of laser enhanced ionization spectroscopy (LEIS).

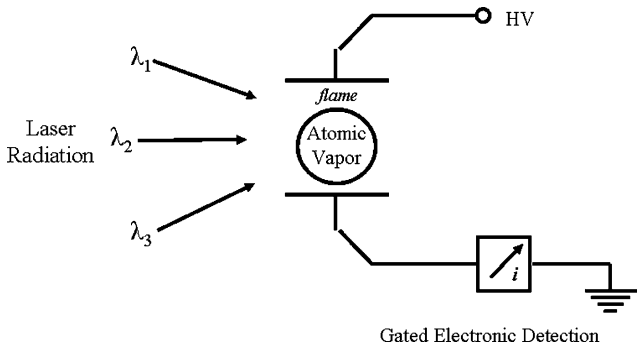

Fig. 10 Schematic representation of resonance ionization spectroscopy (RIS) with field ionization or photoionization. Multiple laser beams are required.

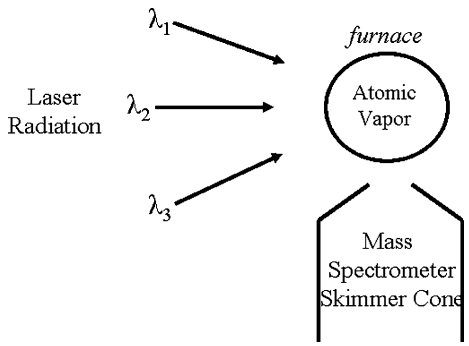

Fig. 11 Schematic representation of resonance ionization mass spectrometry (RIMS) with photoionization. Multiple laser beams are required.

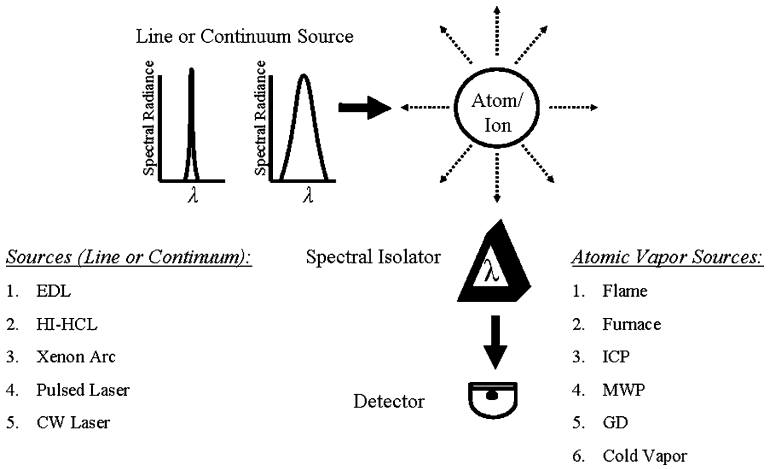

Fig. 8 Schematic representation of atomic fluorescence spectroscopy (AFS) with types of sources and types of atom sources.

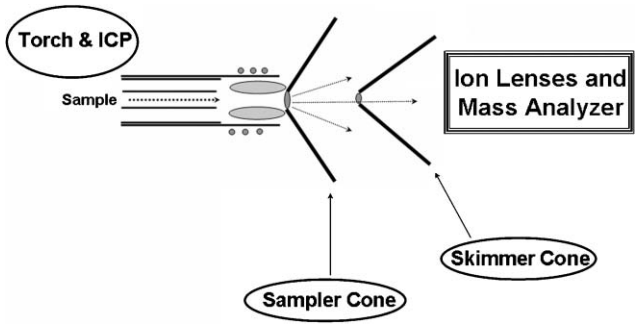

Fig. 12 Schematic representation of inductively coupled plasma (ICP) mass spectrometry (MS). The ICP could be replaced with a pulsed or cw glow discharge or a microwave plasma.

Table 1 Figures of merit (FOM)

Considered	Not considered
Detection power	Similar operating conditions for all elements
Selectivity	Sample preparation
Linear dynamic range	Automation
Single atom detection (SAD) and/or single atom measurement (SAM)	Sample size
	Spatial/temporal resolution
Absolute analysis	Speed and simplicity of analysis
Multielement analysis	Instrument and operating cost
"Age" of method	Instrument compactness
Research activity	Destructive or non-destructive
Application activity	Bulk *versus* surface analysis

The detection power is defined as the reciprocal of the detection limit which has units of grams of analyte per gram of sample. Therefore, a detection power of 10^{12} would correspond to a detection limit of 1 part per trillion. One should not use sensitivity to mean detection power or detection limit. Sensitivity is strictly defined as the slope of the calibration curve.[27]

The selectivity is more difficult to define because it can be divided into at least two major parts. One part is the *spectral selectivity* of the method.[27,32] The spectral selectivity is defined as the intensity of the analyte peak of concern divided by the overlapping wings of close atomic or molecular spectral lines/bands or masses. For example, it is in principle impossible to optically detect a radiocarbon atom, ^{14}C, against the background of ordinary carbon, ^{12}C, atoms since the concentration ratio is 10^{-12} to 10^{-16}. This is despite the well-defined isotopic shift of their spectral lines; the infinitesimal overlapping of the spectral wings limits the minimum concentration of ^{14}C that can be detected against the background of ^{12}C by ordinary spectral means. However, if we use multiple excitation steps (λ_1, λ_2, λ_3...) and/or mass spectrometric measurement of resulting ions, then the overall spectral selectivity, S_o, will be a product of the individual selectivities, S_1, S_2, S_3, ..., namely

$$S_o = S_1 S_2 S_3... \quad (1)$$

and so it is possible to obtain spectral selectivities of 10^{12} to 10^{20}, which means that a single radioactive atom could be detected in 1 mg–1 g of a sample. Since the detection method does not rely on the radioactive decay of a nucleus, it can be applied with similar success to long-lived radioisotopes (half lives of 1–10^6 years) which, in principle, cannot be detected in the preceding concentrations and amounts by any nuclear physics techniques. Therefore, only RIS and RIMS are capable of such high spectral selectivities.[22,24,25] The spectral selectivities of atomic emission techniques (ICP), assuming a high resolution spectrometer, are $\sim 10^4$–10^5, and atomic absorption techniques give S_0 values of $\sim 10^5$–10^7 depending on whether hollow cathode lamps or diode lasers are used.

There is no formally accepted definition of *matrix selectivity*. Kaiser[27] and Fujiwara, *et al.*,[32] attempted to give a formal definition to matrix selectivity but neither approach has been widely used. The matrix selectivity depends upon the sample composition and the means of converting the analyte in the sample to atoms or ions, such as flames, furnaces, plasmas, *etc*. For example, if a given atomic spectroscopic method gives the *same* signal for the same concentration of analyte in all samples for a given set of conditions for converting the sample into atoms and ions, *then* we can say the method has complete matrix selectivity, namely no interferences due to the matrix on the conversion of analyte in the sample to atoms/ions. Several methods well known in the 1960s, such as flame atomic emission spectrometry and flame atomic absorption spectrometry, have to a large extent either died or are rarely used because of poor matrix selectivity as well as wide variation in detection limits for all the elements. However, the dc arc emission spectrometric method is still being widely used despite the presence of significant matrix interferences. Because of the large number of variables and conditions for the sample and the conversion process, matrix selectivity will not be one of the FOM considered here.

The linear dynamic range, LDR, is the ratio of the analyte concentration where the calibration curve drops by 5% from linearity to the limit of detection. Therefore, LDR is a dimensionless number. For hollow cathode-atomic absorption spectrometry, LDR is $\sim 10^2$; however, LDRs can reach 10^5 with diode laser-AAS on AAS and $\sim 10^5$–10^9 with laser fluorescence and laser ionization methods.

As was stated in the Introduction, the "age" of the method, as predicted by the authors, is a modification of the original Laitinen[1] "Seven Ages of an Analytical Method". Laitinen's seven ages were also used by and modified by Fassel[2] and Hieftje.[3,4] The major changes by the present authors include 5 new ages, denoted with asterisks (2*, 3*, 4*, 5*, 7*), where the method could reach senescence or old age, even death, prior to age 7 (Table 2). In addition, analytical spectroscopists would not be aware of those reaching 2* because most of such possible methods would have "died" in the physics literature. There are some other more subtle changes to Laitinen's seven ages" but the reader is referred to his original A-pages article in *Analytical Chemistry*.

The FOM of absolute analysis, single atom detection (SAD), single atom measurement (SAM) and "age" of the method will be discussed in separate sections. The other FOM of multielement analysis, current research activity, and current application activity require no special discussion.

Single atom detection (SAD)/single atom measurement (SAM)

There are laser-based spectroscopic methods for which spectroscopists claim the ability to detect single analyte atoms (or molecules). Laser-based methods in which the sensitivity is sufficiently high (and the noise sufficiently low) to ensure that individual species in the laser beam can be detected are called single-atom detection (SAD) methods.[33–38] This terminology follows the convention established by Alkemade[34] where detected analyte species are collectively referred to as atoms, even though the analyte species may be atoms, molecules, ions or radicals. Techniques capable of SAD can be broadly categorized as using either destructive or non-destructive methods of detection. In the destructive case, the atom is consumed during the detection process (ionization of atoms, for example), producing at most one single event per atom. In the non-destructive case, each atom can produce multiple detectable events during its interaction with the laser (fluorescence, for example). The measurement of a single atom (SAM) is a far more difficult task since not only must the detection method achieve SAD but also the efficiency of production of atoms from the sample, the efficiency of transfer of atoms to the detection region, and the efficiency of probing of the atoms

Table 2 Modified seven ages of an analytical method[a]

Age	Phase
1	Conception of idea
2	Experiments establish validity of principle(s) as basis for measurement.
(2)*	*Senescence (physics).*
3	Instrumental developments result in "method" used by (non)specialist.
(3)*	*Senescence. "Method" dies due to lack of interest.*
4	Detailed studies of principle(s) and mechanisms. "Method" matures.
(4)*	*Senescence. "Method" dies due to lack of interest.*
5	Applications increase to many areas. Publications result.
(5)*	*Senescence. "Method" dies due to lack of interest.*
6	Applications of well-established procedures—"cookbook".
7	Senescence. "Method" is further improved by research and/or other methods surpass the "method".
(7)*	*Senescence. "Method" dies due to lack of interest.*

[a] H.A. Laitinen, *Anal. Chem.*, 1973, **45**, 2305. V.A. Fassel, *Z. Anal. Chem.*, 1986, **324**, 511. G.M. Hieftje, *Spectrochim. Acta (Vatican Issue)*, 1989, **44B**, 113; *J. Chem. Ed.*, 2004, **77**, 579.

must all be unity. The measurement process is depicted more clearly in Table 3.

If SAD is to be possible, each and every atom which interacts with the laser beam in the laser spectroscopic method and within the probe volume V_p must be detected above the background noise. The number of events detected during the measurement time, t_m, are counted. During this time, a certain volume, V_a, of sample containing analyte flows past the laser beam. However, only those atoms within the probed volume have a probability of being detected. Depending on the duty factor for a pulsed laser, *i.e.*, the product of the repetition frequency, f_L, of the laser and the laser pulse duration, t_p ($f_L t_p$), a certain number of atoms, N_p, which enter V_p interact with the laser beam during time t_m. A given atom in V_p interacts with the laser beam for an interaction time, t_i. The atom's interaction time, t_i, is a function of t_m, the type of laser (pulsed, cw, or modulated) and the atom residence time, t_r, in V_p. The value of t_r, the atom residence time in volume V_p, usually varies for different atoms with a mean value of t_r, depending upon factors such as velocity, diffusion, and the size and shape of V_p. The atom's corresponding interaction time, t_i, may also be a variable with a mean of t_i depending on the relative magnitudes of t_m and t_r and the conditions of the experiment.

The detection efficiency, ε_d, of an atom which interacts with the laser beam at the intrinsic detection limit (noise is due only to the variance of the signal itself) is given[33–36] by

$$\varepsilon_d = 1 - \exp(-\phi_s t_i) \text{ (dimensionless)} \quad (2)$$

where ϕ_s (s^{-1}) is the mean flux of signal counts due to the atom in V_p (s^{-1}); it is assumed that there is no noise due to the background. Thus, for SAD, ε_d must be unity. For non-destructive detection, ϕ_s is the mean flux of detected events. For destructive detection, ϕ_s is the reciprocal of the mean detection time once the atom has entered the detection region. For both destructive and non-destructive detection, the number of detected events (counts), N_e, in the measurement time, t_m, is given by

$$N_e = YN_A \text{ (counts)} \quad (3)$$

where N_A is the total number of analyte atoms measured during the atom residence time, t_r, and within the cell volume during t_r, and Y is the sensitivity, counts per atom, for the measurement method. The sensitivity Y is given by

$$Y_{SAM} = \varepsilon_I \varepsilon_V \varepsilon_{a,i} \varepsilon_T \varepsilon_s \varepsilon_t \varepsilon_d \quad (4)$$

where ε_I = sample introduction efficiency, ε_v = sample matrix vaporization efficiency, $\varepsilon_{a,i}$ = efficiency of atom (a) or ion (i) formation, ε_T = transport efficiency to the detection system, ε_s = spatial probing efficiency, ε_t = temporal probing efficiency and ε_d = detection efficiency. All efficiencies are dimensionless. It is easy to understand why SAD could exist but SAM is not possible. For SAD to exist, Y_{SAD} is given by

$$Y_{SAD} = \varepsilon_d \quad (5)$$

Therefore, for a certain laser ionization method, Y_{SAD} could be unity, whereas Y_{SAM} could be 10^{-3}, indicating that only 1 out of 1000 atoms in the sample pass through the detection cell and are detected. This could be solely the result of poor spatial and temporal probing. Methods capable of SAD include most laser fluorescence and ionization methods, whereas, most, if not all, analytical methods are not capable of SAM.

The reader is referred to several previous papers[33,34,36] by the Winefordner group involving the estimation of ε_d, Y_{SAM}, and LODs based on the use of both intrinsic and extrinsic noise sources. However, it is instructive to estimate ε_d, N_e and the LOD for several atomic spectroscopic methods. First, AES in an ICP will have an ε_d given[33] by

$$\varepsilon_d = 1 - \exp(-\eta_{ex} A_{ul} t_r \eta_{em} \eta_{el} \eta_d) \text{ (dimensionless)} \quad (6)$$

where

$$\eta_{ex} = \frac{g_u}{Z(T)} \exp -\left(\frac{E_u}{kT}\right), \quad \text{(dimensionless)} \quad (7)$$

g_u = statistical weight of upper level (dimensionless)
Z(T) = electronic partition function (dimensionless)
E_u = upper level from which emission transition occurs (J)
k = Boltzmann constant (J K^{-1})
T = temperature of plasma (K)
A_{ul} = spontaneous emission transition probability from level u to level l (s^{-1})
t_r = residence time of atom in the observation region(s)
η_{em} = collection efficiency of spectrometric system (dimensionless)
where η_{em} is given by

$$\eta_{em} = \frac{whQ_E T_o}{4\pi A_{em}} \quad \text{(dimensionless)} \quad (8)$$

The terms in η_{em} are given by
w and h = the width (cm) and height (cm) of the optical (spectrometer) aperture (slit)

Table 3 Measurement of single (few) atoms

Conversion process
Atoms in samples present as compounds
Compounds must be converted to atoms
Atoms must be transferred to detector
Detection process
Each atom must produce detector event
Detector event must be detectable above noise

Ω_E = the solid angle of collection (sr)
T_o = overall transmittance of the optical system (dimensionless)
A_{em} = the total emission surface area (cm^2)
η_{el} = efficiency of electronics (counts/photoelectron)
η_d = detection efficiency of photons reaching the detector (photoelectrons/photon).

Reasonable values of parameters[33] for nebulization-ICP-AES are $\eta_{ex} = 3 \times 10^{-16}$ for $\lambda_{ul} = 200$ nm and $T = 6000$ K to $\eta_{ex} = 1 \times 10^{-6}$ for $\lambda_{ul} = 500$ nm and $T = 6000$ K ($g_u/Z(T)$ is assumed to be unity). $A_{ul} = 10^8\ s^{-1}$, $t_r = 10^{-3}$ s, $\eta_{em} = 8 \times 10^{-7}$, and $\eta_{el}\eta_d = 10^{-1}$. Therefore, ε_d goes from 2.4×10^{-18} to 8×10^{-6} counts per atom for $\lambda_{ul} = 200$ nm and $T = 6000$ K and $\lambda_{ul} = 500$ nm and $T = 6000$ K, respectively. Thus, single atom detection and single atom measurement is far from achievable, no matter what the noise sources and no matter how large $\varepsilon_I\varepsilon_V\varepsilon_{a,i}\varepsilon_T\varepsilon_s\varepsilon_t$.

Reasonable values of parameters[33] for LIBS are: $\eta_{ex} \cong 2 \times 10^{-2}$ for $\lambda_{ul} = 500$ nm and $T = 8000$ K and $\eta_{ex} \cong 4 \times 10^{-5}$ for $\lambda_{ul} = 200$ nm and $T = 8000$ K ($g_u/Z(T)$ is assumed to be 1), $t_r = 1 \times 10^{-6}$ s, $\eta_{em} = 6 \times 10^{-6}$ (dimensionless), $A_{ul} = 10^8\ s^{-1}$, and $\eta_{el}\eta_d = 10^{-1}$. Therefore, ε_d goes from 1.2×10^{-7} counts per atom for $\lambda_{ul} = 500$ nm and $T = 8000$ K to 2.4×10^{-9} counts per atom for $\lambda_{ul} = 200$ nm and T = 8000 K. Once again, no matter what the noise process and no matter how large $\varepsilon_I\varepsilon_V\varepsilon_{a,i}\varepsilon_T\varepsilon_s\varepsilon_t$, SAD and SAM cannot be achieved.

However, for the case of single color excitation LEAFS, assuming a 2-level system and under optical saturation conditions, the expression for ε_d is given[33] by

$$\varepsilon_d = 1 - \exp(-gA_{ul}t_p\eta_{fl}\eta_d\eta_{el}) \text{ (dimensionless)} \quad (9)$$

$$g = \frac{g_u}{g_u + g_l} \quad (10)$$

where

$$\eta_{fl} = \text{fluorescence collection efficiency} = wh\Omega_F T_o/4\pi A_{Fl} \text{ (dimensionless)} \quad (11)$$

w, h and T_o are as defined for the emission system, Ω_F (sr) is the solid angle of collection, A_{fl} is the total surface area (cm^2) over which fluorescence occurs, and t_p, η_d and η_{el} have been defined above.

Reasonable values of the parameters are: $g = 1$, $\eta_{fl} = 1 \times 10^{-2}$, $t_p = 10^{-8}$ s, $A_{ul} = 10^8\ s^{-1}$, and $\eta_{el}\eta_d = 10^{-1}$. Under these conditions, ε_d is 0.001 counts per atom and one can see SAD is approached but not achieved.

Finally, for two color laser induced ionization where both transitions are saturated, ε_d is given by

$$\varepsilon_d = 1 - \exp(-g'k_{u'i}t_p\eta_d\eta_{el}) \text{ (dimensionless)} \quad (12)$$

where

$$g' = \frac{g_u}{g_l + g_u + g_{u'}} \quad (13)$$

u' is the level reached by the second excitation step, u is the level reached by the first excitation step, $k_{u'i}$ is the effective collisional rate constant for level u′ into the ionization continuum, i (s^{-1}), and all other terms have been previously defined. Reasonable values of $g' = 1$, $k_{uNl} = 1 \times 10^{10}\ s^{-1}$, $t_p = 10^{-8}$ s and $\eta_{el}\eta_d = 10^{-1}$, result in $\varepsilon_d = 1$ count per atom. Therefore, it is clear that for certain laser ionization experiments, single atom detection and possibly SAM can be achieved as long as the noise sources are reduced to intrinsic noises and $\varepsilon_I\varepsilon_V\varepsilon_{a,i}\varepsilon_T\varepsilon_s\varepsilon_t$ is near unity, which is possible but difficult in some experiments with furnaces.

It is clear that only laser-based techniques, particularly those based on ionization, are capable of SAD and possibly SAM. No other cases will be discussed here. The reader is referred to other papers[33,35,36] for the estimation of ε_d and ε_m. In the section on Resurgence of atomic absorption with diode lasers, further discussion of SAD is given for a method normally considered to be far from the capability of SAD. The need for single atom detection (measurement) can clearly be seen in Table 4, where the determination of lead in sea salt aerosols requires SAD or more particularly SAM, since there will only be about 4 Pb atoms in the laser volume during the detection (measurement) process.

Table 4 Need for single atom detection

Example: Determination of natural Pb level in sea salt aerosols by Flame-LEAFS
$\approx 10^3$ particles cm^{-3}
≈ 1 L min^{-1} flow rate
≈ 0.1 μm particles ($\rho \approx 1$ g cm^{-3})
≈ 0.4 cm^3 laser probing volume
$\approx 1.3 \times 10^{-7}$ Pb fraction ($\varepsilon_v\varepsilon_a = 1$)[a]
≈ 4 Pb atoms in laser volume

[a] ε_v = vaporization efficiency, ε_a = atomization efficiency

Resurgence of atomic absorption with diode lasers

The rate of absorption, R_{lu}, in s^{-1}, is given[19,20] by

$$R_{lu} = \sigma_{max} I_{laser} \frac{\Delta\nu_{eff}}{\Delta\nu_{laser}} \text{ (Hz)} \quad (14)$$

where σ_{max} is the maximum absorption cross section, in cm^2, I_{laser} is the laser intensity in photons s^{-1} cm^2, $\Delta\nu_{eff}$ is the effective absorption half width, in Hz, over the laser profile, and $\Delta\nu_{laser}$ is the laser half width in Hz. The maximum absorption cross section, σ_{max}, is given by

$$\sigma_{max} = 2.65 \times 10^{-2} \frac{f_{abs}}{\Delta\nu_{eff}} \text{ (cm^2)} \quad (15)$$

where f_{abs} is the absorption oscillator strength (dimensionless) and so the absorption rate, R_{lu}, is given by

$$R_{lu} = 2.65 \times 10^{-2} \frac{I_{laser}}{\Delta\nu_{laser}} f_{abs} \text{ (Hz)} \quad (16)$$

For a 2 mW diode laser at 852.1 nm for Cs ($f_{abs} = 0.76$) and with a laser beam area of 0.008 cm^2 and a laser half width, $\Delta\nu_{laser}$, of 20 MHz, $R_{lu} = 1.1 \times 10^{10}$ Hz, which exceeds the deactivation rate of atoms in most cells. This shows that saturation can be easily achieved with modest energies with diode lasers.

Hannaford[39] showed that an ideal atomic absorption experiment would comprise atoms at rest so that only natural broadening occurs and a narrow line diode laser is used, therefore $\Delta\nu_{laser} < \Delta\nu_{eff}$. Under these conditions, from the classical theory of dispersion and pure natural broadening of the atomic absorption lines

$$\sigma_{max} = \left(\frac{\lambda_0^2}{2\pi}\right) \text{ (cm^2)} \quad (17)$$

Therefore, σ_{max} is independent of the absorption oscillator strength, f_{abs}, which gives additional fuel to the use of atomic absorption for absolute analysis as well as SAD. The fraction of radiation absorbed in this special case, α_{abs} is given by

$$\alpha_{abs} = 1 - \exp(-\sigma_{max}n_{abs}L) \xrightarrow{\text{low}\sigma_{max}n_{abs}L} \sigma_{max}n_{abs}L \text{ (dimensionless)} \quad (18)$$

where σ_{max} has been defined above, n_{abs} is the number density of absorbers (cm^{-3}), and L is the absorption path length (cm). Since n_{abs} is related to the total number of absorbers, N_{abs}, by

$$n_{abs} = \frac{N_{abs}}{LA_l} = \frac{N_{abs}}{L\pi r_l^2} \text{ (cm^{-3})} \quad (19)$$

where r_l is the radius (cm) of the laser beam and A_l is the area

Table 5 Minimum fraction absorbed, α, for shot noise limitation and for several diode laser powers[a37]

φ_o/W	α_{shot}
10^{-7}	2×10^{-6}
10^{-5}	2×10^{-7}
10^{-3}	2×10^{-8}
10^{-1}	2×10^{-9}

[a] Note: $\eta = 0.8$ A/W and $\Delta f = 1$ Hz.

(cm^2) of the laser beam. In terms of absorbance, A, at low absorbancies this is given by

$$A = 0.434\alpha_{abs} = 0.434\sigma_{max}n_{abs}L \text{ (dimensionless)} \quad (20)$$

$$A = \frac{0.434\sigma_{max}N_{abs}}{\pi r_l^2} = \frac{0.434\lambda_0^2 N_{abs}}{2\pi^4 r_l^2} \approx 2\times10^{-2}\,\frac{\lambda_0^2}{r_l^2}N_{abs} \text{ (dimensionless)} \quad (21)$$

If $r_l = 10$ μm and λ_0 is any wavelength between 200 and 800 nm, N_{abs} will be less than 1 for a minimum absorbance, A_{min} of 10^{-4} or smaller, which is possible with wavelength modulation or frequency modulation assuming the shot noise limit.

If σ_{max} is determined by collisional and Doppler broadening, and $\sigma_{max} \sim 10^{-15}$ cm^2, then N_{abs} will exceed 1 atom depending upon λ_o and the limiting S/N. Therefore, it is clear that atomic absorption spectrometry is an elemental technique with possible LODs approaching or surpassing the LODs of most other atomic spectroscopic methods. Nevertheless, the technique is still basically a single element method which certainly detracts from such possible detection powers. By means of an echelle spectrometer and a xenon arc source, atomic absorption spectrometry becomes a multielement detection method with good LODs but certainly results in LODs much higher than those discussed above.

Another way of looking at the limiting detectable fraction absorbed in atomic absorption spectrometry,[40] especially with stable diode laser sources, is to assume the signal is limited by shot noise which results in

$$\alpha_{shot} = (n_{abs}\sigma_{max}L)_{shot} = \sqrt{\frac{2e\Delta f}{\eta\phi_0}} \text{ (dimensionless)} \quad (22)$$

where e is the charge of an electron (1.6×10^{-19}C), Δf is the electrical measurement frequency bandwidth, Hz, η is the detector responsitivity, A/W, and ϕ_0 is the incident radiation power, W. In Table 5, the minimum value of α_{shot} for several diode laser powers are given (η is taken as 0.8 A/W and $\Delta f =$ 1 Hz). It should be stressed that these values of α_{shot} are seldom achieved because the detected unabsorbed light carries excess low frequency noise, called flicker or $1/f$ noise. Therefore, in principle, if the shot noise limitation can be reached, then it should be possible to measure α values as small as 10^{-9} (or even 10^{-13} to 10^{-14}—see next section), which could allow limits of detection approaching single atom detection. In order to achieve the shot noise limit, modulation techniques must be used, especially frequency modulation (see next section); wavelength modulation alone will not achieve the shot noise limit. Double modulation, wavelength plus the sample, will improve the detection limit but still not achieve the shot noise limit and result in α as low as $\sim 10^{-7}$.

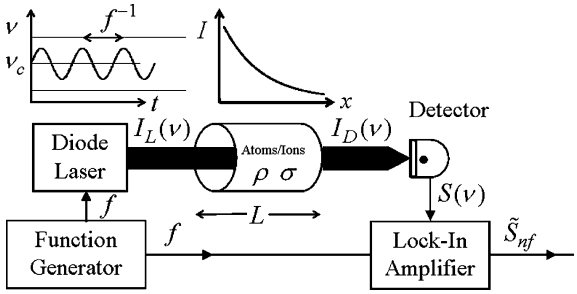

Fig. 14 Typical schematic diagram for wavelength modulation diode laser atomic absorption spectroscopy.

Modulation methods

Wavelength modulation (principles represented in Fig. 13) has been used in virtually every area of spectroscopy, but by far its greatest use has been in atomic absorption spectrometry. Axner *et al.*,[41] published an extensive review on wavelength (and frequency) modulation absorption spectrometry. Wavelength modulation atomic absorption spectrometry, together with diode lasers, has been evaluated by many researchers but certainly the most extensive work has been done by Niemax's group[42,43] and Axner's group.[41,44,45] A typical experimental setup for wavelength modulation is given in Fig. 14.

Wavelength modulation (WM) and frequency modulation (FM) differ with respect to the relation between the amplitude and frequency. Certainly WM is simpler, more rugged, and more used than FM. Laser based absorption methods can

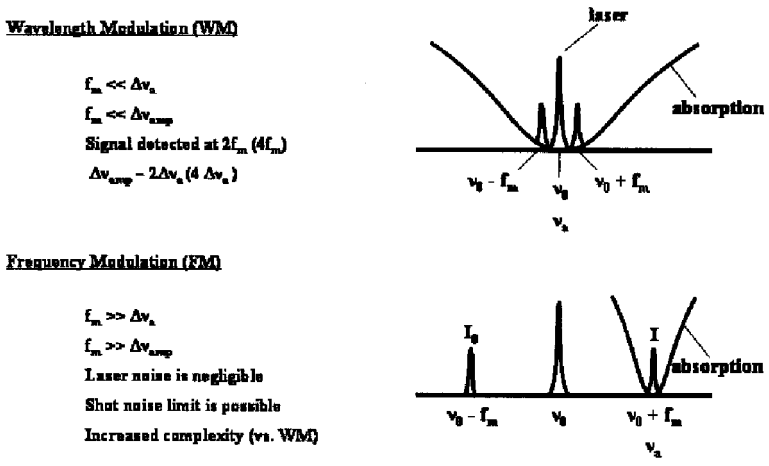

Fig. 13 Representation of the principles of wavelength and frequency modulation.

benefit from WM (and FM) primarily because absorption methods are based upon measuring the difference between two large signals, which involves measuring the detection signal in the presence and absence of the analyte (on and off resonance). With diode lasers, this is accomplished by either moving on and off resonance or by continually tuning the wavelength over the resonance. The high detection power of WM atomic absorption spectroscopy is based on a smooth modulation at frequency f_m of the wavelength (often in the kHz–MHz range) followed by detection of the signal at a certain harmonic of f_m, namely nf_m (n = 2,3,4,*etc*). Detection capability is at a higher frequency, where $1/f$ noise, which dominates at low frequencies, is significantly smaller. The drawback of WM atomic absorption is that the signal is not a simple replica of the traditional absorption spectra; in fact, many WM spectra have only a vague resemblance to the spectra responsible for the absorption of light. In addition, it is more difficult for an experimentalist to know when the method is optimized.

If the frequency of modulation, f_m, is much smaller than the half-width of the absorption profile, $\Delta\nu_a$, the resulting signal is the nth derivative of the lineshape function and so the method is called derivative spectroscopy. Axner, *et al.*,[40,44,45] reviewed in detail the analytical expressions for arbitrary harmonics of the WM absorption signals from Lorentzian, Gaussian, and Voigt absorption profiles and for a variety of absorption and instrumental conditions.

Frequency modulation (FM) is similar to WM but here the frequency of modulation is sufficiently high that $f_m \gg \Delta\nu_a$ and so the condition shown in Fig. 13 applies. In other words, the sidebands, at ν_o (the central frequency of the laser) $\pm f_m$, are shifted sufficiently far from ν_0 that the absorption line (band) at a frequency of ν_a is peaked at $\nu_0 + f_m$, $\nu_0 + f_m$ and $\nu_0 - f_m$ are separated so far, it is possible to measure the absorption of the analyte at $\nu_0 + f_m$ (I is intensity transmitted through the sample) and the background absorption at $\nu_0 - f_m$ (I_0 is the intensity transmitted through the "perfect" blank). Frequency modulation does not result in any modulation of intensity at the modulation frequency, f_m, in the absence of absorbers. Modulation of the intensity at the modulation frequency, f_m, is produced by beating between the carrier frequency and one of the sidebands. However, since the amplitudes of the sidebands are equal, there will be a perfect cancellation of the signal at the modulation frequency. At such a high modulation frequency, virtually all flicker noise has an amplitude below the shot noise. Unfortunately, frequency modulation spectrometry (FMS) does not generally reach the shot noise limit due to laser excess noise, etalon fringes, and other technical noise sources. Certainly, if all technical noise sources are removed, the shot noise limit could be achieved by FMS. Despite its advantages, FM is seldom used by analytical spectroscopists because of the additional complexities.

Cavity ringdown absorption spectrometry has reached α values of 10^{-6} or lower. In the case of using a superstable Nd:YAG laser (1 Hz) locked to a cavity with a finesse of 10^5, α of 10^{-10}–10^{-11} have been obtained. Unfortunately, the instrumental demands are high.

Cavity enhanced frequency modulated absorption spectrometry involves the use of a Fabry–Perot cavity for low light and highly reflecting mirrors to achieve a finesse, $F = 10^5$. By modulating the laser light at a high frequency equal to the free spectral range of the cavity, noise is cancelled because the noise is the same on all three modes of the laser (sidebands and main band).[40] This technique is called noise-immune cavity enhanced optical heterodyne molecular spectroscopy, NICE-OHMS,[46,47] but has not yet been applied to practical analytical problems. However, α values of 10^{-13}–10^{-14} should be possible. Again, the instrumentation is rather complex (see Fig. 15).

Absolute analysis

In spectrochemical analysis, and generally in all analytical methods, the functional dependence of the variable c (analyte concentration) or q (analyte amount) upon a physical parameter X, the signal, has the form

$$X = f(c) \text{ or } X = f(q) \tag{23}$$

If a theoretical expression is known for the function $f(c)$ or $f(q)$ that is sufficiently reliable to allow a direct calculation of c (or q) from a single blank corrected measurement in absolute units of the physical quantity represented by X, then and only then can we speak of an absolute analysis.[27] This is the only acceptable definition of absolute analysis, *i.e.*, the capability of providing quantitative results without the use of standard reference materials. Therefore, the idea of chemically isolating the analyte from the matrix so that the analysis can be performed by simple comparison with standard aqueous solutions cannot be placed in the context of absolute analysis.

It is worthwhile to stress the difference between *absolute* and *standardless* analysis. Some methods of chemical analysis can be made sufficiently stable with time and reproducible so that known reference materials need to be used only infrequently; Kaiser[27] referred to such a stability as *fixed*, f, calibration. The fixed calibration approach may be referred to as *standardless* analysis while *absolute* analysis requires detailed and reliable knowledge of the theoretical relationships between analyte concentration, c, or mass, q, and the measured signal. In other words, Kaiser's[27] so-called *perfect*, p, calibration, where the analytical procedure must be described in every detail, will ultimately result in an estimate of analyte mass without the need to resort to any standard materials.

In the past, the possibility of performing an absolute analysis has usually been considered by analytical chemists as a dream.[26] This is understandable if one considers the complex

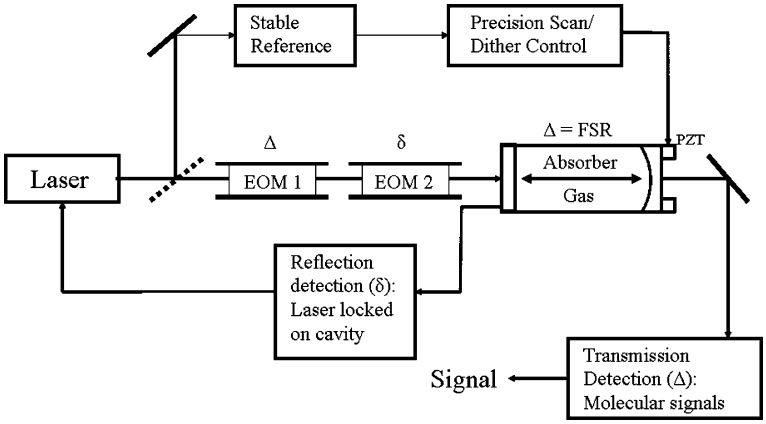

Fig. 15 Schematic diagram of NICE-OHMS.[35] Experimental setup.

Table 6 Possible uses of absolute elemental analysis

Heavy metals (Tl, Pb, Cd, *etc.*) in old Antarctic snow and ice layers (levels below 10–13 g g^{-1})[60–62]
Quantization of natural radioactive impurities in an ultra-clean liquid scintillator (U at ~10–16 g g^{-1})[63,64]
Determination of trace elements in samples of interest in criminalistic and forensic medical cases[65]
Distribution of elements (attogram levels) on surfaces
Analysis of ultra-pure materials in semiconductor industry[66]
Analysis of hazardous species as radioactive Pu in natural water and soil samples
Analysis of elemental composition of single particles, *e.g.*, atmospheric aerosols[67–72]

chemical, physical, and instrumental aspects of an overall analytical procedure which involves sample preparation and atomization (ionization), the mechanism of excitation and de-excitation, and the characteristics of the electro-optic detection systems.

Mandelstam and Nedler[48] examined the problem of calculating the sensitivity of emission spectrochemical methods and determined that accurate quantitative calculations were not practical. Both Walsh[49] and L'vov[50] recognized early on that atomic absorption spectrometry could be an absolute method and De Galan[51,52] was probably the first to provide a detailed examination of absolute analysis using a spectrochemical method, namely the dc arc. Boumans[53] also gave the theoretical foundation of the dc arc spectrochemical method. In 1968, Rann[54] gave a thorough treatment of absolute analysis using flame atomic absorption and De Galan and Samaey[55] compared flame atomic emission and flame atomic absorption as absolute methods. However, the major approach to analytically useful absolute analysis has been treated by L'vov[56] for electrothermal atomization-atomic absorption spectrometry. L'vov's[56–58] group compared theoretical and experimental characteristic masses of 40 elements. Other workers have expanded on these studies. There have been few studies involving absolute analysis by spectroscopic methods other than ETA-AAS. The Winefordner, Omenetto and Smith group submitted two proposals (not funded) to a federal agency involving absolute analysis by ETA-LEAFS (electrothermal atomization-laser excited atomic fluorescence) and by ETA-laser enhanced ionization in a flame; however, no publications on either approach have appeared. Palleschi, *et al.*,[59] have described a calibration free approach for LIBS (laser-induced breakdown spectroscopy).

In all of these methods, variations in the analyte amount (concentration) detected differed by about 10–20% from the known amount (concentration). Some possible unique uses of absolute analysis are given in Table 6.

Comparison of atomic spectroscopic methods

Using the major figures of merit listed in Table 1 and the biases of the authors, the atomic emission, atomic absorption, atomic fluorescence, atomic ionization, and several other lesser known atomic methods are compared in Tables 7–14 to the three major techniques (ICP-AES, ICP-MS, and ETA-AAS). In order for the tables to be reasonable in size and content, only one of the three major techniques is listed in each table; namely, the major technique closest to the group being compared.

Table 7 Atomic emission spectroscopy (AES) figures of merit

Method	Detection power	Selectivity	LDR	SAD (SAM)	Absolute analysis	Multi-element	Age	Research activity[a]	Application activity[a]
Inductively coupled plasma (reference)	3	2	3	No (No)	No	Yes	7	>	≫
Flame	2	2	2	No (No)	No	Yes?	7	≪	≪
Arc	2	2	2	No (No)	Yes	Yes	7	≪	=
Spark	1	1	1	No (No)	No	Yes	7	≪	=
Microwave plasma									
-induced	2	2	2	No (No)	No	Yes	7	=	=
-surface wave	2	2	2	No (No)	No	Yes	5*	<	<
-torch	2	2	2	No (No)	No	Yes	5*	<	<
-capacitative	1	2	2	No (No)	No	Yes	5*	<	<

[a] Poor, ≪, 1; Fair, 2, <; Moderate, 3, =; Good, 4, >; Excellent, 5, ≫.

Table 8 Atomic emission spectrometry (AES) figures of merit

Method	Detection power	Selectivity	LDR	SAD (SAM)	Absolute analysis	Multi-element	Age	Research activity[a]	Application activity[a]
Inductively coupled plasma (reference)	3	2	3	No (No)	No	Yes	7	>	≫
Laser microprobe (LIBS)	1+	2	2	No (No)	No (Yes?)	Yes	4	≫	≫
Graphite furnace	2	2	2	No (No)	No	No	3*	≪	≪
Furnace atomization plasma (FAPES)	3	2	2	No (No)	No	Yes	3+	<	<
Furnace atomic non-thermal excitation spectroscopy (FANES)	4	2	3	No (No)	No	Yes	3+	<	<

[a] Poor, ≪, 1; Fair, 2, <; Moderate, 3, =; Good, 4, >; Excellent, 5, ≫.

Table 9 Atomic emission spectroscopy (AES) figures of merit

Method	Detection power	Selectivity	LDR	SAD (SAM)	Absolute analysis	Multi-element	Age	Research activity[a]	Application activity[a]
Inductively coupled plasma (reference)	3	2	3	No (No)	No	Yes	7	>	≫
Glow discharge dc	2	2	2	No (No)	No	Yes	7	=	=
Glow discharge rf	2	2	2	No (No)	No	Yes	5	=	=
Glow discharge pulsed	2	2	2	No (No)	No	Yes	5	<	<

[a] Poor, ≪, 1; Fair, 2, <; Moderate, 3, =; Good, 4, >; Excellent, 5, ≫.

Table 10 Atomic absorption spectroscopy (AAS) figures of merit

Method	Detection power	Selectivity	LDR	SAD (SAM)	Absolute analysis	Multi-element	Age	Research activity[a]	Application activity[a]
ETA (HCL) (reference)	*4*	*5*	*2*	*No (No)*	*Yes*	*No*	*7*	$\gg$	$\gg$
ETA (Xe)	2	2	3	No (No)	Yes?	Yes	7	$<$	$<$
Flame (HCL)	2	2	2	No (No)	No	No	7	$\ll$	$<$
Cold vapor (HCL)	4	4	2	No (No)	Yes	No	7	$\ll$	$>$
ETA (Flame)–diode laser									
-wavelength modulation (WM)(DL)	4	5	5	No (No)	Yes	No	5	$=$	$=$
-frequency modulation (FM)(DL)	4	5	5	Yes (No?)	Yes	No	4	$=$	$\ll$

[a] Poor, $\ll$, 1; Fair, 2, $<$; Moderate, 3, $=$; Good, 4, $>$; Excellent, 5, $\gg$.

Table 11 Other atomic absorption spectrometry (pulsed laser source) figures of merit

Method	Detection power	Selectivity	LDR	SAD (SAM)	Absolute analysis	Multi-element	Age	Research activity[a]	Application activity[a]
Cavity ringdown (flame)	4	5	3	Yes? (No)	Yes?	No	3	$<$	$\ll$
Multipass (flame)	4	5	3	Yes? (No)	Yes?	No	3*	$<$	$\ll$
Intracavity (flame)	5	5	3	Yes? (No)	Yes?	No	1	$\ll$	$\ll$
CFS/AMORS	3	3	2	No (No)	Yes?	No	4*	$<$	$\ll$
NICE-OHMS	5	5	5	Yes (No?)	Yes?	No	1	$=$	$\ll$
Atomic photothermal spectrometry	?	?	?	No (No)	No	No	1	$\ll$	$\ll$

[a] Poor, $\ll$, 1; Fair, 2, $<$; Moderate, 3, $=$; Good, 4, $>$; Excellent, 5, $\gg$.

Table 12 Atomic fluorescence spectrometry (AFS) figures of merit

Method	Detection power	Selectivity	LDR	SAD (SAM)	Absolute analysis	Multi-element	Age	Research activity[a]	Application activity[a]
Flame–EDL/HCL	3	5	4	No (No)	No	No	5*	$\ll$	$\ll$
Flame–Xe arc	2	3	3	No (No)	No	Yes	5*	$\ll$	$\ll$
ETA–EDL/HCL	3	5	4	No (No)	No	No	4*	$\ll$	$\ll$
Glow discharge–EDL/HCL	1	5	2	No (No)	No	No	4*	$\ll$	$\ll$
Cold vapor–EDL/HCL	4	5	3	No (No)	No	No	7	$=$	$\gg$
HCL–ICP	3	5	4	No (No)	No	No	5*	$\ll$	$\ll$

[a] Poor, $\ll$, 1; Fair, 2, $<$; Moderate, 3, $=$; Good, 4, $>$; Excellent, 5, $\gg$.

Table 13 Atomic fluorescence spectrometry (AFS) figures of merit

Method	Detection power	Selectivity	LDR	SAD (SAM)	Absolute analysis	Multi-element	Age	Research activity[b]	Application activity[b]
Laser excitation (LE)[a] –Flame	4	5	5	No (No)	No	No	3*	$\ll$	$\ll$
LE–ETA[a]	5	5	5	Yes? (No?)	Yes?	No	4	$=$	$<$
LE–ICP[a]	3	4	4	No (No)	No	No	3*	$\ll$	$\ll$
LE–Glow discharge[a]	3	4	4	Yes? (No)	Yes?	No	4*	$\ll$	$\ll$
LE–atom beam/atom trap[a]	5	5	—	Yes (No)	Yes?	No	1	$=$	$<$

[a] Major use: Diagnostics of flames, gases, plasmas; n_a's, n_i's, n_e's, k's, φ's. [b] Poor, $\ll$, 1; Fair, 2, $<$; Moderate, 3, $=$; Good, 4, $>$; Excellent, 5, $\gg$.

Table 14 Atomic ionization spectrometry (AIS) figures of merit

Method	Detection power	Selectivity	LDR	SAD (SAM)	Absolute analysis	Multi-element	Age	Research activity[b]	Application activity[b]
ICP-MS (reference)	5	4	5	No (No)	No	Yes	7	$\gg$	$\gg$
Flame-LEIS[a]	4	2	4	No (No)	No	No	7	$<$	$\ll$
Furnace–RIMS[a]	5	5	5	Yes? (No)	Yes?	No	5*	$<$	$<$
Furnace–RIS[a]	5	4	5	Yes? (No)	Yes?	No	5*	$\ll$	$\ll$

[a] Major use: diagnostics of flames, gases, plasmas; n_a's, n_i's, n_e's, k's, φ's. [b] Poor, $\ll$, 1; Fair, 2, $<$; Moderate, 3, $=$; Good, 4, $>$; Excellent, 5, $\gg$.

Concluding remarks on the comparison of methods

The (personally biased) evaluation given in the various tables is self-explanatory. It therefore allows the reader to draw a conclusion about the performance of the various techniques given and therefore to rank them in order of such performance. *The validity of this exercise is clearly limited to the figures of merit chosen in Table 1*. On that basis, the big three methods, ETA-AAS, ICP-AES and ICP-MS, are superior to most other analytical atomic spectroscopy methods.

The above limitation is intrinsic to any attempt to put different methods on a comparative basis. Needless to say, if the chosen criterion would have only been detection power and spectral selectivity for a certain element, or cost and portability,

or temporal resolution in diagnostic experiments, the three superstars would have been surpassed by other methods among those considered.

Highlighting LIBS

History

The development of laser induced breakdown spectroscopy (LIBS) and understanding of laser induced plasmas (LIP) are directly related to advances in lasers (Table 15).[73] After the stimulated emission was predicted by Einstein in 1917, it took more than 40 years to build the first ruby laser.[74,75] In 1962, the ruby laser was used by Brech[76] to produce vapors from metallic and non-metallic materials. The vapors were then excited by an auxiliary spark source and emission spark spectra were detected. This experiment was the birth of LIBS. Remarkably, most of this early work dealing with LIP was carried out using a delayed electrical spark for formation of the spectrochemical plasma.

In 1964, Maker *et al.* first used LIP not only as a sampling tool but also as an emission source.[77] Analytical curves for nickel and chromium in steel samples were constructed based on the emission detected directly from the LIP. From that moment, LIBS became a technique for direct spectrochemical analysis.

In the same year, 1964, it was predicted by Basov and Khrokhin that LIP could be used for nuclear fusion.[78] This caught the attention of many theorists and led to the extensive theoretical exploration of LIP. The first theoretical model for laser breakdown of a gas was developed in 1965 by Zel'dovich and Raizer.[79] Six years later, in 1971, the first comprehensive monograph was published by Ready which summarized both theoretical and experimental investigations of LIP and LIBS.[80]

Since then, interest in spectroscopic applications of LIP, *i.e.* LIBS, has closely correlated with instrumental developments. After the first wave of enthusiasm in the early 1970s, when a few commercial instruments were manufactured (most notably by Jarrell–Ash Corporation and VEB Carl Zeiss), the interest in LIBS slowly declined towards the end of the decade. The LIBS instrumentation was expensive and unreliable, while the analytical performance of LIBS could not even distantly compete with other modern analytical techniques, like electrothermal atomization atomic absorption spectrometry (ETA-AAS) or inductively coupled plasma-atomic emission spectrometry (ICP-AES).

The renewed interest in LIBS came in the middle of the 1980s, along with the availability of reliable, small and inexpensive lasers and, more importantly, with the development of sensitive imaging optical detectors, such as the intensified charge-coupled device (ICCD). These detectors, allowing time-resolved spectral measurements in a wide spectral window, perfectly matched with the needs of spectrochemical LIBS analysis. It was immediately recognized that the unique advantages of LIBS, such as the capability for rapid, *in situ*, multi-element analysis of any kind of sample with no sample preparation, could be integrated into a new generation of analytical techniques. This understanding triggered many new LIP diagnostics and theoretical studies.

At this time, LIBS remains a very active field. LIBS is used for fast and easy compositional analysis of solids, liquids, gases and aerosols; it is widely applied for thin film deposition; it may simulate atmospheric lightening and stellar processes.[6,81,82] Commercial LIBS instrumentation is now appearing on the market. Efforts are being made to push this technology toward miniaturization and further minimization of cost. The potential applications include detectors for hazardous materials (biological and chemical agents, land mines, *etc.*) in prescribed locations, forensic analysis at crime scenes, environmental monitoring and space exploration.

Fundamentals

Formation and evolution of LIP in different media. The details of laser induced breakdown depend greatly on the medium, on the environment and on the laser being used. A major point in the LIP initiation is the production of seed electrons. According to a standard definition, the breakdown occurs when a density of free carriers (electrons) reach approximately $\sim 10^{18}$ cm^{-3}, which provides strong optical absorption in the plasma.[83] The mechanism of the production of seed electrons depends strongly upon the aggregate state and the material type. As opposed to the laser induced desorption (or "cold ablation") which may involve only point-like matter–light interaction, the laser breakdown (or "hot ablation") is the collective phenomenon which involves material bulk properties, such as elasticity, compressibility, *etc*. The bulk properties also determine mechanisms of energy deposition and dissipation which occur on a typical ablation length scale. The ablation length scale can be estimated from the relationship $d = \tau_{\mathrm{laser}}\, v_{\mathrm{s}}$, where τ_{laser} is the duration of a laser pulse and v_{s} is the speed of sound in the material. This relationship determines not only the ablation size, but also reflects the fact that the processes leading to ablation (excitation, thermalization, lattice instability, *etc.*) are "driven" by the laser pulse for its entire duration.[84] Below, a brief description is given of how the plasma is formed in different media (Table 16).

1. Gases. The initial electrons are created by cascade or multiphoton ionization. Also, at high irradiances ($\geqslant 10^{12}$ W cm^{-2}), the tunnel effect can contribute where electrons are pulled out of atoms by the laser field through the potential barrier of electrostatic attraction.

For cascade ionization to start, at least one electron should be present in an irradiated volume. This electron may come as a result of cosmic ray ionization or a micro-breakdown of a gas impurity. After the electron gains sufficient energy *via* inverse bremsstrahlung,[85] impact ionization of other atoms occurs and the cascade starts leading to an exponential growth of the number of electrons.

Multiphoton ionization occurs as a result of simultaneous absorption of several photons provided that the sum energy of

Table 15 Historical development of laser induced plasmas (LIP) and laser induced breakdown spectroscopy (LIBS)

When	Who	What
1917	Einstein	First theorized about "stimulated emission", the process which makes lasers possible
1958	Shawlow, Tawns	Theorized about a visible laser
1960	Maiman	Built first ruby laser with optical pumping
1962	Brech, Cross	Birth of LIBS: detection of spectrum from ruby laser induced plasma
1964	Runger *et al.*	First direct spectrochemical analysis by LIBS
1965	Zel'dovich, Raizer	First theoretical model for laser breakdown of a gas
1971	J.F. Ready	First monograph summarizing developments in LIP/LIBS
1970s	Jarrell–Ash, Carl Zeiss	First commercial LIBS
1980s	Companies/research labs	Better lasers, ICCD gated detectors, renewed interest in LIBS
1980s–present	Research labs/companies	Expansion of LIP/LIBS applications and theoretical modeling

Table 16 Summary of laser–matter interaction and LIP evolution

Media/properties	Medium excitation/seed electron formation	Energy dissipation	Plume formation	Plume development
Gases High ionization energy (>10 eV)	Multiphoton and cascade ionization; tunneling	Ionizing, elastic, inelastic collisions; electron attachment	Heating electrons (inv.bremmstrahlung); photoionization	Expansion of electrons and highly ionized atoms; shock wave; laser light absorption; formation of luminous plasma. Decay through radiative, quenching, and electron-ion recombination, formation of clusters, diffusion of species into ambient gas.
Liquids "effective" conduction and valence bands	Multiphoton and cascade ionization; shallow donors excitation	Collisions, recombination, trapping in solvated states, diffusion	Inv. bremmstrahlung, ionizing collisions; explosive nucleation, cavitation	
Metals Small bandgap, ~zero electron–lattice coupling	Direct electron heating; surface plasmon excitation.	Electron scattering from lattice ions, thermal diffusion	Vaporization at the melt front; phase explosion; electronic sputtering;	
Semiconductors Small-moderate bandgap, weak electron–lattice coupling	Formation of electron-hole plasma; transverse optical phonons excitation	Electron-hole recombination, thermal heating of the lattice	hydrodynamic sputtering	
Insulators Large band gap, strong electron–lattice coupling	Multiphoton excitation of valence band electrons	Electron-phonon scattering; photomechanical effects (spallation)		

the photons is higher than the ionization potential of an atom. This process is only important at short wavelengths because ionization potentials of most gases are high ($\geqslant 10$ eV) while the probability of simultaneous absorption quickly decreases with the number of photons required for ionization. Therefore, multiphoton ionization can dominate cascade ionization only at short wavelengths or low densities.

2. Liquids. A sequence of processes leading to breakdown in liquids is less theoretically understood than that in gases or solids. The amorphous nature of liquids, the variation in the localized potential seen by the quasi-free electron, the tendency of liquid molecules to associate in clusters in an undetermined manner, all make electron mobility in liquids highly complex.[83,86] Nevertheless, experimental measurements in liquids show field dependence similar to that found in solids. Therefore, liquids are often treated as amorphous solids with effective conduction and valence bands and the formation of seed electrons is described by cascade and multiphoton ionization, common for both gases and solids.

Once created, the plasma is heated far beyond the vaporization point by inverse bremmstrahlung, resulting in explosive nucleation and cavitation. A dense vapor-cavity zone is formed in the subsurface region followed by violent vapor-plume ejection and shock wave propagation after the termination of the laser pulse. The upward vapor-plume ejection imposes recoil momentum on the liquid surface causing its deformation. In this stage, the intense hydrodynamic motion is activated generating bulk-liquid ejection, which mainly occurs as the result of work done by collapsing cavitation bubbles.[87]

3. Solids. In metals, the nearly free conduction-band electrons absorb laser photons by direct heating of the electron gas. Electron–lattice coupling (the degree to which ion motion follows electron motion in a solid) is essentially zero; the electrons provide dielectric screening of the lattice ions and prevent them from directly interacting with light. The laser induced excitation is dissipated *via* collisions between excited electrons and the lattice, *i.e.* thermal conductivity.

In semiconductors and insulators, both electrons and ions contribute to the excitation. There are no free conduction-band electrons in insulators and only a few in semiconductors. Thus, optical absorption (*via* multiphoton band-to-band transitions) leads to the creation of electron-hole pairs rather than electron heating. Only at very high irradiances ($\sim$TW cm^{-2}) is it possible to create a significant number of conduction-band electrons and generate free-electron heating. Strong electron–lattice coupling plays a definitive role in energy dissipation; relaxation mechanisms include electron-hole recombination and response of the lattice to the creation and motion of free charges and electron-hole pairs.[84]

Despite the differences in LIP initiation in different media, the subsequent plasma evolution is similar. The ablated material in the form of free electrons and highly ionized atoms expands at a velocity much faster than the speed of sound and forms a shock wave in the surrounding atmosphere. During laser action, the expanding plume continues to absorb energy from the laser beam and forms a luminous plasma. After several microseconds (up to tens of microseconds), the plasma plume slows down *via* collisions with ambient gas species, whereas the shock wave detaches from the plasma front and continues propagating at a speed approaching the speed of sound. Finally, the plasma starts to decay through radiative, quenching and electron–ion recombination processes that lead to formation of high density neutral species in the post-plasma plume. The decay ends with formation of clusters (dimers, trimers, *etc.*) *via* condensation and three-body collisions and with thermal and concentration diffusion of species into the ambient gas. This usually occurs within hundreds of microseconds (up to milliseconds) after the plasma has been ignited.

The general physical picture can be modified greatly in the regime of a femtosecond pulse ablation.[84,88,89]

Plasma modeling. In recent years, many workers have modeled laser breakdown in solids, liquids and gases. The increasing number of theoretical publications reflects the impressive progress which has been made in understanding the fundamental mechanisms governing laser induced plasmas, both in terms of laser–material interaction and the post-breakdown plasma evolution.

A simple model of laser–metal interaction was proposed by Lunney and Jordan,[90] where a single absorption cross-section was assigned to both atoms and ions to account for bound–bound and bound–free transitions. The model was used to calculate plasma absorption, average ion energy, and ablation depth for an iron target irradiated with an excimer laser. Callies and colleagues[91] investigated the UV-ablation mechanism. For UV-lasers, the effect of inverse bremsstrahlung was shown to play a minor role due to a strong laser shielding caused by Mie absorption on condensed clusters. Yalçin *et al.*[92] studied the influence of ambient conditions on the laser air spark and found evidence in support of a laser-supported radiation wave model. Hermann *et al.*[93] developed a model of a non-uniform plasma divided into two uniform zones of different densities and temperatures to describe self-absorption of the plasma radiation. Casavola *et al.*[94] analyzed non-equilibrium conditions during a laser induced plasma expansion by coupling fluid dynamic and kinetic equations. In further studies by the same authors,[95] the fluid dynamic equations were coupled with the chemical equilibrium model to predict the temperature and time-dependent density profiles. Itina *et al.*[96] modeled the expansion of a laser plume into vacuum or background gas by using the gas dynamic approach followed by the Direct Monte Carlo Simulation. The model explained the formation of a shock wave and described the reactive interaction between the plume and the gas species. Ho *et al.*[97] simulated the dynamics of a laser plasma using the one-dimensional model of target heating combined with two-dimensional radiative gas dynamics. The authors discussed in detail plasma radiation effects.

A kinetic approach was used by Mazhukin *et al.*[98] to simulate the time-dependent energy distribution of atoms and ions. The model described optical breakdown induced by a UV laser in an Al vapor. Basic mechanisms of non-equilibrium ionization of Al vapor were analyzed and the dominant effect of photo-processes on the distribution of plasma species was shown. Mazhukin *et al.* have also contributed two other papers[99,100] dealing with the mathematical modeling of laser plasmas initiated in different media. Mazhukin *et al.*[99] described plasma dynamics at the air–water interface by the system of gas-dynamic equations and the radiative transfer equation. It was shown that plasma evolution strongly depended on the laser wavelength and that plasma radiation contributed significantly to the redistribution of plasma energy. Mazhukin *et al.*[100] studied the effect of radiative transfer on gas dynamics of an Al laser plasma. The mathematical description included two-dimensional radiation gas dynamics and the multi-group diffusion approximation for plasma radiation transfer. Calculation of the plasma spectrum was performed for wide (0–100 eV) and narrow (optical, 2–5 eV) energy windows.

Experimental verification of theoretical models has been realized by measuring various plasma properties and comparing them against predicted ones. Among plasma properties, the luminous, spectral properties are of primary importance as they are easily measurable and carry rich information about the plasma structure and composition. Thus, plasma spectral measurements provide a powerful feedback to correct and verify a theoretical plasma model. The model itself, if complete, should predict detailed spectral distribution of radiation. Regretfully, there are only a few models in the literature which allow spectral calculations. Meanwhile, such a model is in a great demand for spectroscopy and for analytical spectroscopy, in particular, since it may help in achieving the ultimate goal of absolute analysis in analytical spectroscopy.

Our group has recently contributed two papers in which relatively simple models of laser induced plasmas were proposed aiming at application in practical spectroscopy. In the first paper,[101] a simplified theoretical approach was developed for an optically thick inhomogeneous LIP. The model described the time evolution of the plasma continuum and specific atomic emission after the laser pulse had terminated and interaction with a target material had ended. Calculations were performed for a two-component Si/N system. The model predicted spatial and temporal distributions of atom, ion and electron number densities, evolution of atomic line profiles and optical thicknesses, and the resulting absolute intensity of plasma emission in the vicinity of a strong non-resonance atomic transition (Fig. 16). Practical applications of the model included prediction of temperature, electron density, and the dominating broadening mechanism. The model could also be used to choose the optimal line for quantitative analysis.

In the second paper,[102] we expanded the semi-empirical model proposed in the previous publication.[101] A radiation dynamic model of a post-breakdown plasma expanding into vacuum was developed. The model was based on a system of gas dynamic equations coupled with the equation of radiative transfer. Calculations were performed for a dual SiC system, although calculations for any arbitrary number of system's components were also permitted. The model predicted the evolution of plasma temperature, the spatial and temporal distributions of atoms, ions and electron number densities and the evolution of the plasma spectrum in a desirable spectral window (*e.g.*, 280–290 nm for the chosen in this work SiC system, Fig. 17). The model solved a two-fold problem. First, it yielded an analytical expression for the plasma radiation dynamics (and the synthetic spectra) under arbitrarily chosen initial conditions. Second, the developed computational routine allowed finding the initial conditions by a direct comparison of calculated synthetic spectra with experimentally measured spectra. The model provided a rather simple theoretical means to link the observed spectral features, such as the intensity and the shape of spectral lines to the plasma composition. In this respect, it was considered as a step toward the possibility of performing absolute analysis.

Calibration-free LIBS. Absolute analysis is the ultimate goal of many spectrochemical methods as it permits eliminating matrix effects (especially pronounced in LIBS) and avoiding a tedious calibration procedure which usually requires matrix-matched standards. Recently, a new procedure was proposed by Ciucci *et al.*,[103] allowing calibration-free quantitative LIBS analysis of materials. The procedure was based on detecting spectral lines from all sample constituents in a wide spectral window and constructing a family of Boltzmann plots corresponding to all constituents. Constituent concentrations could then be calculated from the intercepts of the Boltzmann plots with the y-axis drawn in the so-called Boltzmann plane ($\ln(I_\lambda/g_kA_{ki})$ *versus* E_k, where I_λ is the measured line intensity, g_k, A_{ki} and E_k are the statistical weight, the transition probability and the upper level energy, respectively. The method has been successfully applied to analysis of an aluminium alloy (Fig. 18) and atmospheric air.

Later, the procedure was corrected for possible line self-absorption.[104] The curve-of-growth approach was used to estimate the degree of self-absorption for all lines and to calculate Lorentzian line widths. The iterative algorithm was used to compute line intensities as if non-linear effects were absent. The new procedure was applied to certified steel standards and gave reliable results, improving the precision and the accuracy of

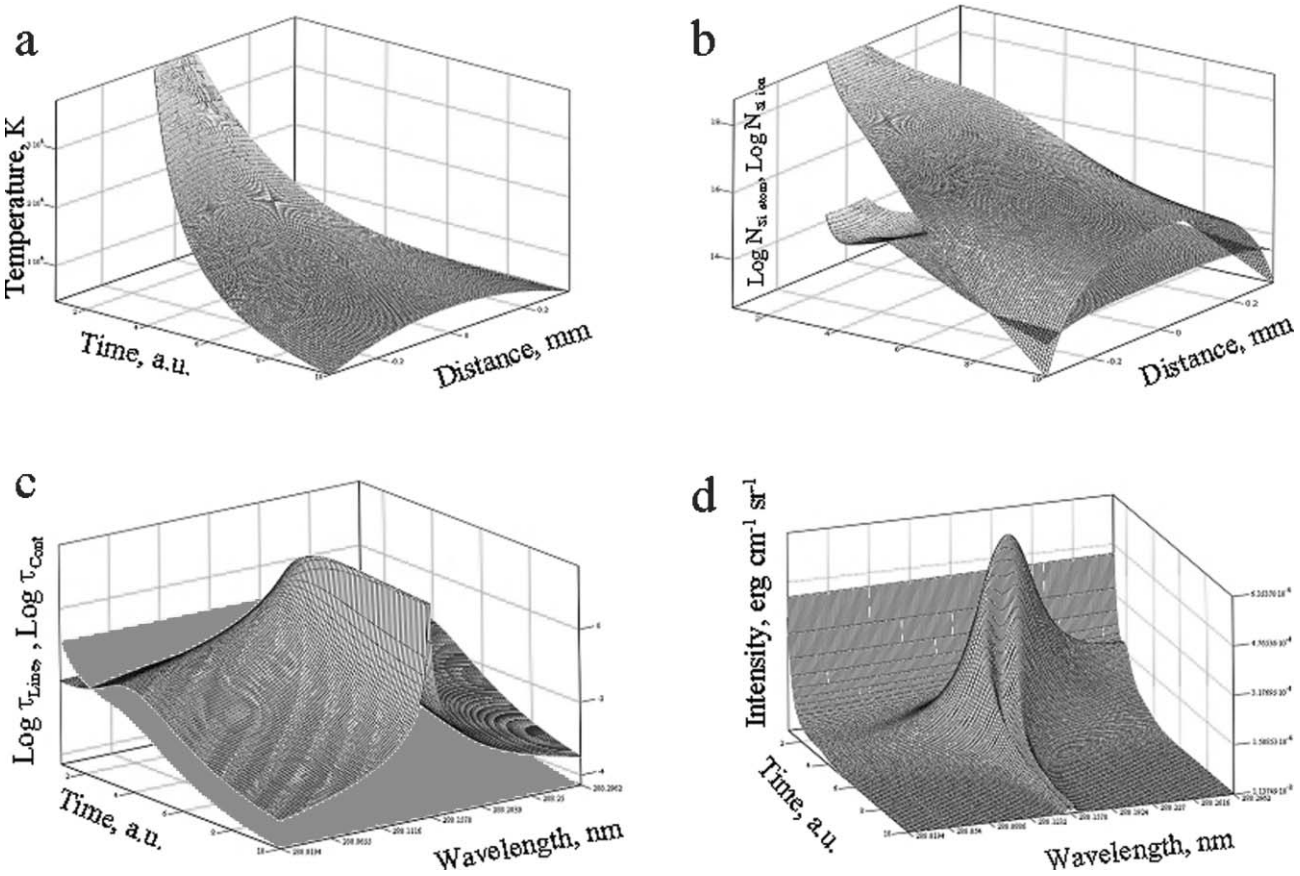

Fig. 16 Surface plots representing some of the computed plasma parameters for the plasma consisting of 1016 atoms with the Si/N ratio equal to 0.01. (a) Time and space evolution of the plasma electron temperature; (b) the electron density with respect to the lower level Si atom density as the function of space and time; (c) the optical depth of the continuum with respect to the optical depth of line absorption as the function of time and wavelength; (d) the resulting emission intensity as the function of time and wavelength.

calibration-free analysis by one order of magnitude compared with the previous procedure in reference.[103]

Instrumentation and importance of laser characteristics

Typical LIBS set-up. Typical instrumentation includes an ablation laser, an optic collection system, a spectral filter (a conventional grating monochromator or an Echelle spectrometer) and an array detector (typically, an intensified CCD) connected to the computer (Fig. 19). The most crucial element in a LIBS spectrometer is the laser as it determines the character of laser–material coupling and directly affects the behavior of the resulting plasma. Below, we briefly review the effect of laser parameters on plasma formation and development.

High *versus* low energy lasers. The most common terms for describing the laser light are the fluence (J cm^{-2}) and the irradiance (W cm^{-2}). Although the laser fluence is sometimes used as a measure of the breakdown threshold,[105] the situation with plasma initiation is generally more complicated and the breakdown threshold shows a convoluted dependence on both pulse energy and pulse duration. Indeed, the breakdown threshold, defined as the minimum irradiance per pulse required to produce a given number of electrons at the end of the pulse (*i.e.*, a given degree of ionization of the medium) scales differently according to the main mechanism of electron production.[85] In the case of breakdown dominated by multi-photon ionization, the number of electrons produced for a given laser fluence depends upon $[(\tau_p)^{m-1}]^{-1}$, where τ_p is the duration of the laser pulse and m is the number of simultaneously absorbed photons which cause ionization. For example, a low energy, 10 μJ per pulse, laser with a 0.5 ns pulse duration will be 20-fold less effective in production of electrons than an equal power (20 kW) irradiance laser with 0.2 mJ pulse energy and a 10 ns pulse duration. These considerations imply that low power lasers, because of their low pulse energy (and correspondingly low fluence) may well not be capable of producing sample breakdown even at high irradiances.

The effect of laser energy and pulse duration near the breakdown threshold was investigated by Rieger *et al.*[106] In this work, emission from microplasmas induced on Al and Si targets by 50 ps and 10 ns KrF laser pulses (248 nm) was studied in the 0.1–100 μJ range of pulse energies. The emission lifetime of these microplasmas was much shorter (~10–100 ns) than that from plasmas induced by conventional lasers with 10–100 mJ pulse energies (~10–100 μs). It was demonstrated that for energies higher than 3 μJ (and higher than needed for the breakdown of Al or Si), the effect of the pulse width (50 ps or 10 ns) on the plasma emission was minimal, both in terms of emission line intensities and emission lifetimes. In this regime (>3 μJ), the total deposited energy (equal for 50 ps and 10 ns pulses) was more important than the deposition rate (different for 50 ps and 10 ns pulses).

In general, the ablated mass and the mass ablation rate increased with increasing the laser irradiance to a certain point (~1 GW cm^{-2} for a copper target).[107,108] Beyond this point, at higher power densities, plasma shielding effect caused saturation in mass removal at constant ablation rate. Also, at higher laser irradiances higher plasma temperatures were reached, which allowed a higher degree of dissociation and excitation thus improving the analytical sensitivity.

Effect of wavelength. The laser wavelength strongly affects the formation of LIP with respect to both creation of initial

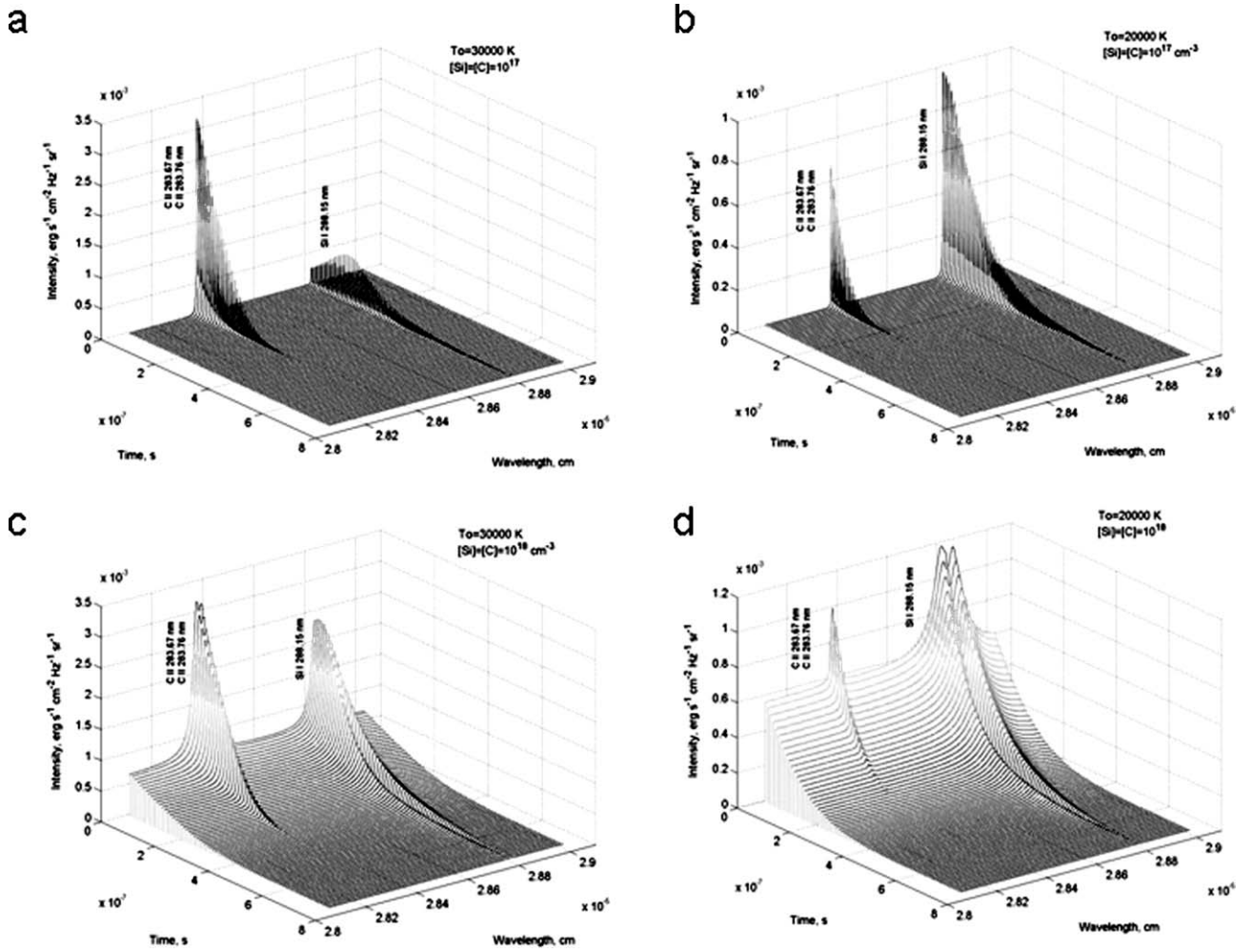

Fig. 17 Surface plots representing the full evolution of the spectra at discrete times of 15 ns and 150 ns, using different initial temperatures and initial concentrations.

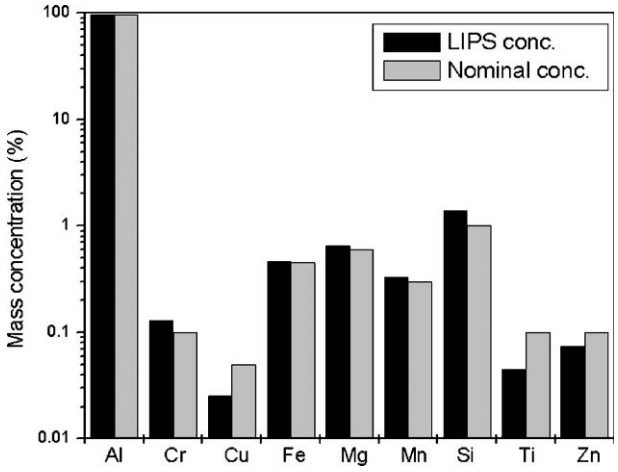

Fig. 18 LIPS quantitative analytical results for an aluminium alloy (anticorodal), compared with the elemental composition declared by the producer. It must be noted that the nominal value for Cu and Ti are only given by the producer as upper limits (adapted from ref. 103).

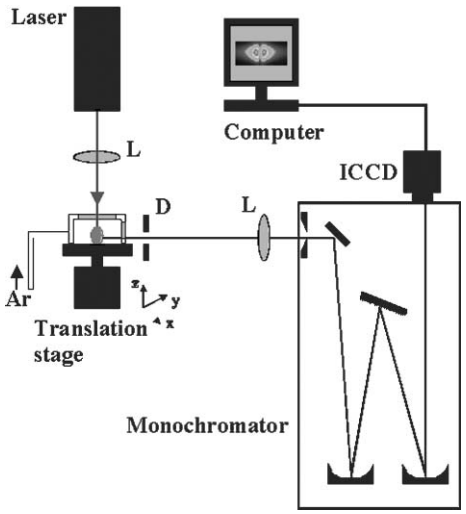

Fig. 19 Typical experimental arrangement for LIBS.

electrons and plasma–laser interaction. Concerning plasma initiation, only short laser wavelengths (UV) produce multi-photon ionization whereas longer (IR) wavelengths are favorable for cascade breakdown (the cascade breakdown threshold scales as λ^{-2}).[85]

Cabalin and Laserna[105] studied the effect of laser wavelength on the ablation threshold for metals with different thermal properties (from Zn to W). Three harmonics (1064 nm, 532 nm, and 266 nm) from a 5 ns pulse width Nd:YAG laser were used. The fluence threshold (J cm^{-2}) was shown to be the lowest for longer wavelengths of 1064 nm and 532 nm, whereas the energy threshold was the lowest for the shortest wavelength of 266 nm. This result agreed with the fact that cascade-like growth of the electron number density due to inverse bremsstrahlung is considerably more favorable in the IR than in the UV (λ^2-dependence). Fluence threshold correlated reasonably well with thermal properties such as melting and boiling points at all

three wavelengths used. Gonzalez *et al.*[109] compared 193, 213 and 266 nm laser ablation of glass standard samples. They found that all three UV wavelengths produced similar ablation behavior, except for the difference in ablation rates. Motelica-Heino[110] studied fractionation effects (the enhancement or depression of elemental species in the vapor phase relative to the bulk) at 1064 and 266 nm and found that fragments of 1–10 μm in diameter were characteristic of IR-ablation of refractory elements (Ca, Al), whereas only submicron particles were characteristic of UV-ablation. For volatile elements (Pb, As, B, Cs), fractionation was found to be significant for both wavelengths (to a greater extent for IR).

Effect of pulse duration. Much attention has recently been paid to the ultra-short laser–material interaction. In contrast to the nanosecond or microsecond scale interaction, the interaction in a femtosecond to picosecond time scale has non-thermal nature.

For metals, the interaction has three interesting limits, depending on the ratio of cooling times for electrons (τ_e) and ions (τ_i) to the duration of the laser pulse τ_p.[84,111] For femtosecond ablation (Fig. 20a), in the limit $\tau_p < \tau_e < \tau_i$, the electrons are not in thermal equilibrium with the lattice by the end of the laser pulse. The energy deposited in the lattice (in delocalized phonon modes) exceeds the critical thermodynamic temperature, resulting in instantaneous evaporation without passing through a melting phase. For picosecond pulses (Fig. 20b), when $\tau_e < \tau_p < \tau_i$, the electrons thermally equilibrate with the lattice during the laser pulse, and the morphology of the ablated surface is determined by competition between melting, vaporization and solidification. Finally, for nanosecond pulses (Fig. 20c), when $\tau_e < \tau_i < \tau_p$, the material is ejected in both vapor and liquid phase. A thermal wave, propagating into the material adjacent to the volume where laser light is absorbed by the plasma, creates a characteristic corona around the crater.

The experimental demonstration of ablation mechanisms in metals was carried out by Sallé *et al.*[112] using the interaction of laser pulses (wavelength 800 nm, pulse durations 70 fs, 150 fs, 0.4 ps, 0.8 ps, 2 ps, 10 ps) with copper in air. As expected, for the femtosecond regime, laser-heated electrons with a temperature several orders of magnitude higher than the surface lattice temperature did not have sufficient time to exchange energy with the lattice during the laser pulse. The authors suggested that the laser energy is transmitted to the matter by electron diffusion driven by a high temperature gradient. They observed that ablation and crater formation took place after the laser pulse. In the picosecond regime, surface evaporation started during the laser pulse; a part of the laser energy was absorbed by the plasma (due to inverse Bremmstrahlung and photoionization) and the amount of laser energy reaching the surface correspondingly decreased. This resulted in lower ablation efficiency compared with femtosecond ablation.

For dielectrics, Perry *et al.*[113] showed that with the use of a femtosecond laser, the initial electrons are formed by multiphoton ionization, which contributes a relatively greater fraction of the electron density as compared with impact ionization which is dominant for longer pulses. In the femtosecond regime, energy from the laser was delivered very fast and the electron heating rate was much greater than the rate of energy transfer to the lattice. Therefore, the damage site was limited to only a small region where the laser intensity was sufficient to produce a plasma with no collateral damage. This process enabled high precision machining of all dielectrics.

Obviously, there has been technological motivation to study damage thresholds in wide-bandgap dielectrics. To give one example, Lenzner *et al.*[114] reported that optical breakdown in fused silica is dominated by avalanche ionization down to the 10-fs regime, whereas for even shorter pulses, multiphoton and tunnel ionization prevailed. They also found that reproducibility of ablation increased dramatically in this 10-fs regime. This was explained as being a direct consequence of the strongly increased deterministic seed electron production by means of multiphoton ionization. More details on theoretical and practical aspects of the short- and long-pulse ablation can be found in recent reviews.[84,115]

Effect of repetition rate and multiple pulses. There are several reasons for using multiple-pulse LIBS. First, the probing efficiency (bulk or surface mass removal) can be substantially increased if high repetition rate laser ablation is used. Second, in a dual- or multiple-pulse regime, where the separation between the laser pulses is shorter than the plasma lifetime, a significant increase in detection sensitivity may result due to the enhanced plasma excitation combined with the increased mass removal.

St-Onge *et al.*[116] investigated plasmas created by a Nd:YAG laser in a double-pulse mode on the surface of Al alloy and found the considerable enhancement in line intensities compared with the intensities obtained in a single pulse mode with equal pulse energy. Plasma temperature and electron number densities measured in both regimes showed, however, only a small (within 10%) difference. The line enhancement, therefore, was attributed to a larger volume of emitting gas and a larger ablated mass. Stratis *et al.*[117] proposed a dual-pulse ablation scheme where a so-called pre-pulse parallel to the target surface created an air plasma above the surface, whereas a second pulse, delayed by a few microseconds, orthogonal to the surface and passing through the air spark, was used for ablation. In this scheme, the ablated mass and spectral line intensities were significantly increased compared with the single-pulse ablation mode. Lapczyna *et al.*[118] used an ultra-high repetition rate (133 MHz) pulse train for precise machining of aluminium. The pulse train was a 2 μs burst of ~250 mode-locked pulses from a Nd:glass laser with a pulse duration of 1.2 ps and pulse separation of 7.5 ns. The burst provided a new mode of laser fluence delivery combining long-pulse heating with the advantages of ultra-short laser–material interaction. Clean craters with minimal traces of melting were obtained. The absence of substantial melt debris was explained by the fact that ultra-fast laser pulses have the advantage of evaporative cooling over a hydrodynamic time scale of the expanding plume, as the locally heated material vaporizes and expands away from the solid, decoupling from it thermally. Much of the heat impulse of an

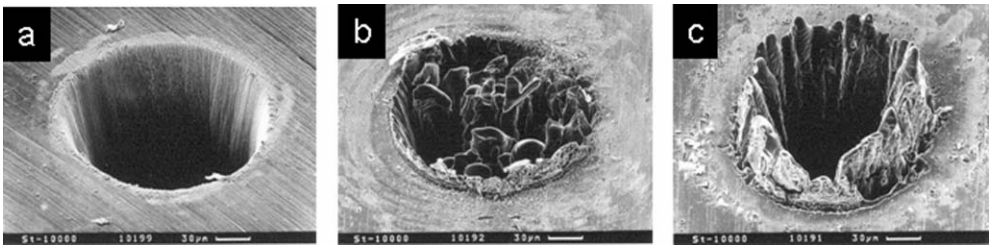

Fig. 20 SEM photographs of holes drilled in a 100 μm thick steel foil with (a) 200 fs, 120 μJ, $F = 0.5$ J cm^{-2} laser pulses at 780 nm; (b) 80 ps, 900 μJ, $F = 3.7$ J cm^{-2} laser pulses at 780 nm; (c) 3.3 ns, 1 mJ, $F = 4.2$ J cm^{-2} laser pulses at 780 nm (adapted from ref. 111).

ultra-fast laser pulse was carried away with the plasma producing etching similar to material sublimation.

Microchip lasers in LIBS. In recent years, efforts are being made to push LIBS technology towards miniaturization and minimization of cost because many LIBS applications aim at mobile field instruments rather than at bulky laboratory setups. In this respect, the newly developing microchip lasers, especially passively Q-switched lasers, can be very beneficial for portable LIBS applications as they combine a miniature size and low power consumption with excellent optical properties, such as single-mode output, low pulse-to-pulse amplitude variation, high beam quality, short pulse width ($\sim$100 ps), and high repetition rate ($\sim$10 kHz).[119] Tight beam focusing, even at moderate pulse energies ($\sim$10 μJ), yields high values for irradiances (GW–TW cm^{-2}) and fluences (1–10 J cm^{-2}) which are sufficient for breakdown of solids.

Our group has investigated the feasibility of using the first commercial 7 μJ microchip laser in LIBS.[120] We found that the plasma induced by the microchip laser was short-lived with duration comparable with the duration of the laser pulse. The plasma continuum background was negligible, allowing usage of non-gated detectors. Due to the low peak power, tight laser focusing with a microscope objective was essential. Such a tightly focused laser was capable of removing 0.5–20 ng mass per pulse from metal foils and a silicon wafer (Fig. 21a). This mass was sufficient to yield spectra detectable with portable grating spectrometers with non-gated non-intensified detector arrays (Fig. 21b).

Applications

Modern applications of LIBS encompass a great variety of fields underlining the unique features of the technique, such as operational simplicity, no sample preparation, applicability to all phases (solid, liquid, gaseous), and relatively low cost. Commercial LIBS instruments are now appearing on the market, although the demand is still low. This can be explained by the lack of methodological and procedural developments which distinguish well established techniques, such as, for example, ETA-AAS or ICP-AES. However, the growing tendency is obvious towards the profound LIBS characterization and standardization which will ultimately convert LIBS

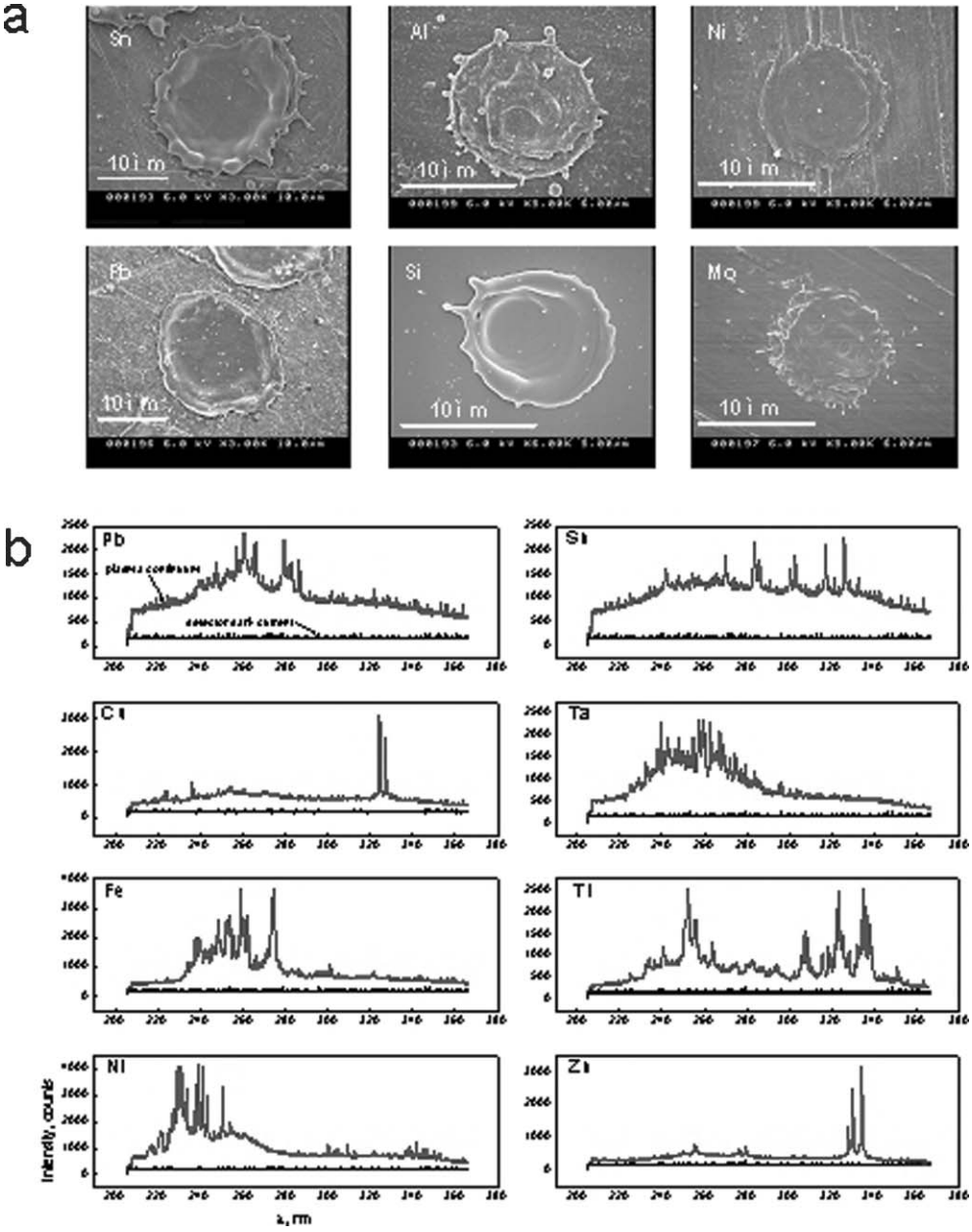

Fig. 21 (a) SEM images of single-pulse craters produced by the 7 μJ microchip laser; (b) spectra obtained with the USB 2000 Ocean Optics spectrometer with a 500 ms integration time. From ref. 120.

Table 17 LIBS applications

Applications	Difficulties	Possible solutions	Figures of merit	Achievements
Analysis of solids	Severe matrix effect	Using matrix-matched standards, different normalization techniques, multivariate calibration, using fs-lasers	Moderate sensitivity (~ppm) and precision (5–10% RSD)	Multielement *in situ* analysis of all types of solid materials in point and standoff detection mode
Analysis of liquids and suspensions	Low plasma excitation; significant fraction of laser energy is converted to mechanical energy	Tilted angles of laser incidence; dried solutions on substrates; dual-pulse LIBS; using fs-lasers	LODs in low percentage –high ppm range	Multielement analysis of aqueous, technological solutions, melts, and biological fluids
Analysis of gases	High breakdown threshold	Using powerful lasers, tight focusing	LODs in low-to-high ppm range	Multielement analysis including "difficult-to-analyze" gases like F, Cl
Analysis/sizing of aerosols	Low probing efficiency with low rep. rate lasers; strong variation in emission signal	Increasing repetition rate, discriminating "null" spectra	Particle concentrations in $\mu g\ m^{-3}$ range; absolute LODs in fg range	Multielement analysis of micron- and sub-micron particles and bioaerosols

into a routine technique. Below, we present a short overview of some interesting LIBS applications obtained with laboratory equipment (Table 17).

Analysis of solids. The vast majority of LIBS applications deal with solid samples. Except for a few preliminary studies,[103,104] quantitative analysis relies upon a carefully chosen calibration procedure. However, in many matrices calibration is difficult and therefore routine quantitative analysis is still elusive because of matrix effects.

The problem of matrix effects has been addressed in many publications. Eppler *et al.*[121] studied the effects of chemical speciation and matrix composition on Pb and Ba detection in soil and sand samples using LIBS. Both factors, the form of chemical compound (carbonate, oxide, sulfate, chloride, or nitrate) and bulk sample composition (different proportions of soil and sand in a soil/sand mixture), were found to strongly influence emission signals. Chaleard *et al.*[122] quantified optical emission signals and corrected for matrix effects assuming emission lines to be a function of two parameters: the vaporized mass and the plasma excitation temperature. The ablated mass was accounted for by using an acoustic signal, whereas the excitation temperature was measured by the two-line method. It was demonstrated that normalization of the net emission intensity by both the acoustic signal and the temperature allowed for a multimatrix calibration curve with about 5% precision for Cu and Mn in various alloy matrices.

In our recent paper,[123] we proposed a matrix-free calibration procedure for quantitative analysis of finely powdered samples. The essence of the method was the normalization of emission intensities by surface densities of analyzed materials provided that the material layer within the laser beam diameter was entirely vaporized. The unique calibration plot was produced using various certified materials (in our case different NIST standards) (Fig. 22). This approach helps to significantly minimize the problem of finding matrix-matched standards which are usually necessary for precise and accurate LIBS analysis.

Typical limits of detection for the analysis of solids by LIBS are in the low-ppm range with typical uncertainty 5–10%. For hybrid techniques, like LA-ICP-MS, the sensitivity can be improved by several orders of magnitude. Shuttleworth and Kremser,[124] for example, used an LA-ICP-sector field mass spectrometer to obtain impressively low detection limits at the ppt level for a large number of elements in glass.

Analysis of liquids. Analysis of liquids by LIBS offers several advantages compared with a standard techniques (like ICP-AES). No sampling for subsequent laboratory analysis is needed; monitoring various elements in liquids including molten metals is possible in real time. These possibilities are in great demand for industrial applications.

Berman *et al.*[125] carried out spectrochemical analysis of aqueous solutions of nickel or chlorinated hydrocarbons using 355 nm or 1064 nm laser radiation focused on the liquid surface. The limits of detection for Ni in water were 18 mg L^{-1} and 36 mg L^{-1} for 355 nm and 1064 nm, respectively. No detectable traces of chlorine were observed even in saturated

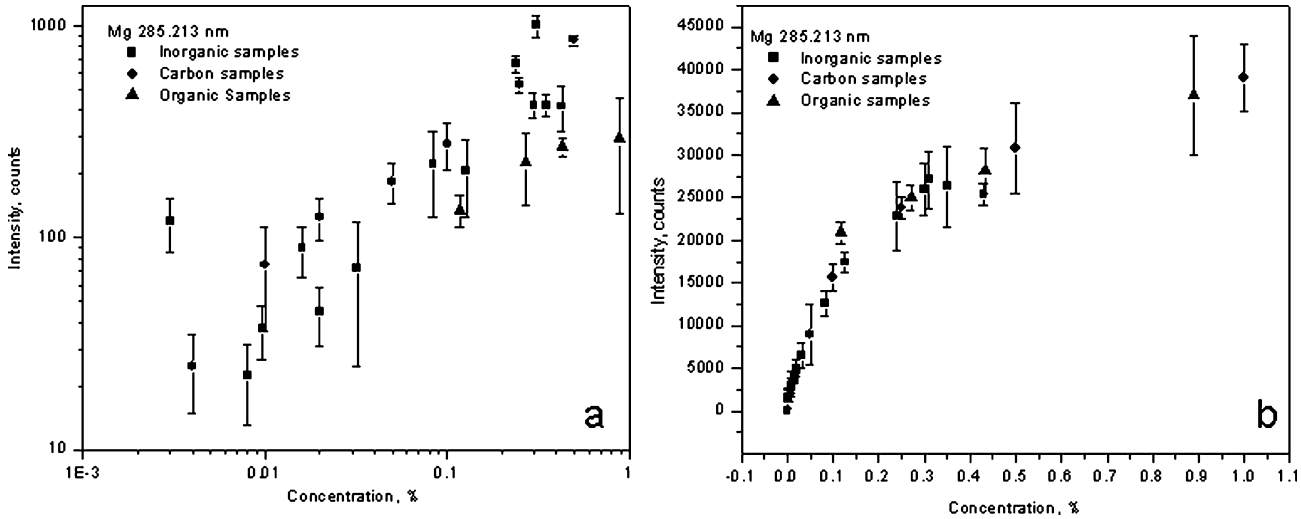

Fig. 22 (a) Untreated data points; (b) surface density-normalized calibration plot. From ref. 127.

aqueous solutions. Fichet *et al.*[126] analyzed traces of 12 elements (Pb, Si, Ca, Na, Zn, Sn, Al, Cu, Ni, Fe, Mg, Cr) in water and oil for use in nuclear applications. A laser (532 nm, 1 Hz) was focused at a tilted angle on the liquid surface providing direct elemental detection without perturbation. No significant differences were observed between the results obtained for oil and water samples. Detection limits, 0.3–120 μg mL^{-1}, and reproducibilities, 3%, were reported.

In general, direct analysis of liquids by LIBS yields very modest sensitivities, typically in the low percentage level. This can be explained by poorer laser–surface coupling than in solids and the conversion of a significant fraction of laser energy (up to 90% of absorbed energy) into mechanical energy[127,128] (a high pressure shock wave, cavitation bubbles). This fraction is smaller for femtosecond lasers (15%), justifying their use in LIBS analysis of liquids. However, under carefully chosen conditions, sensitive analysis of liquids with nanosecond lasers is sometimes possible, as demonstrated by A. Kuwako *et al.*[129] Using dual-pulse LIBS, they were able to detect 0.1 ppb of Na in the aqueous solution of NaCl.

Analysis of gases and environmental monitoring. The detection of trace elements in gases emitted by industrial and incinerator facilities is very important for public health. LIBS seems to be a relevant technique as it combines a continuous monitoring option with the possibility to remotely access a desirable testing site.

Dudragne *et al.*[130] used LIBS for the quantitative detection of F, Cl, S, and C, the usual components of hazardous compounds, in air. The spark was induced in a gas mixing chamber by a Nd:YAG laser at 1064 nm and emission of the elements was detected in the visible and the near-IR. Limits of detection were 20, 90, 1500, and 36 ppm for F, Cl, S, and C, respectively, with ~10% RSD. Partial molecular formulae could be determined by comparing stoichiometric molecular ratios with ratios of calibration plot slopes. H. Zhang *et al.*[131] developed a mobile LIBS system for multimetal continuous emission monitoring. The system successfully measured concentrations of toxic metals (Cr, Pb, Cd, Be) in nearly real time.

Analysis/sizing of particles and aerosols. Particles are playing an ever-increasing role in a wide variety of fields and there is a pressing need for accurate real time characterization methods. For particle analysis, the parameters of interest include size distributions, number densities, and species composition. Based on recent publications,[132–135] LIBS proved to be a suitable technique for the detection of particles and aerosols, with resulting spectra subsequently analyzed for both species composition and total particle mass and size.

Hahn[132] used LIBS for sizing and elemental analysis of aerosol particles in the air. A two-part calibration scheme was developed which established the LIBS system response to a known mass concentration (μg m^{-3}) and a known discrete particle mass. The characteristic plasma volume was then determined, and the overall procedure allowed for the quantitative analysis of the mass and elemental composition of individual, sub-micrometre to micrometre-sized aerosol particles. The extension of the LIBS technique for the quantitative analysis of individual aerosol particles was summarized in ref. 133 using well-characterized calcium-based and magnesium-based aerosols. Aerosol size distributions were recorded using the LIBS technique and using an independent, commercially available measurement technique based on laser light scattering. Histograms of the measured particle size distributions for calcium hydroxide aerosols are presented in Fig. 23 for the two measurement techniques. The light scattering-based sizing data are in excellent agreement with the mass-based LIBS data for both the shapes of the size distribution and the modal diameter. In ref. 135 data are reported for ambient air aerosols containing Al, Ca, Mg and Na for a 6-week sampling period

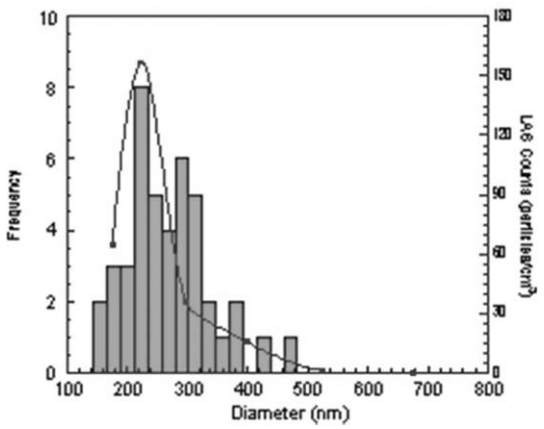

Fig. 23 Histogram of the size distribution recorded for calcium-based particles using the single particle LIBS-based analysis. The continuous curve is the size distribution recorded for the same particle stream using a commercial light scattering instrument. Adapted from ref. 133.

spanning the Fourth of July holiday period. Measured mass concentrations of the elements ranged from 1.7 ppt to 1.7 ppb, with a noticeable increase of Al and Mg (the firework ingredients) during the holidays.

Spatial and depth profiling. Accurate depth profiling is important in many technological fields, including coatings, the production of microelectronic circuits, *etc*. The LIBS technique is well suited for this task as it can provide both the lateral resolution (tight laser beam focusing) and the depth resolution (a regime of low-fluence, gentle ablation).

Margetic *et al.*[136] used a femtosecond laser for depth profiling of Cu–Ag and TiN-TiAlN multi-layers on silicon and iron substrates. Sandwiches of two and three Cu–Ag layers of 600 nm thickness were measured in Ar. No melting or mixing of the Cu and Ag was observed. The ablation rate varied in the range of 10–30 nm per pulse for the laser fluence of 0.5–1.51 J cm^{-2}. The TiN-TiAlN double layers were investigated by LA-TOF-MS and a spatial resolution 10 nm per pulse was achieved. García *et al.*[137] reported that the ablation rate was lower than 2 nm per pulse using a combination of collimated beam ablation and angle-resolved measurements. The angle of incidence of the laser (XeCl) could be adjusted for 0° to 60° while the emission was always collected at a 45° angle with respect to the incident beam. Cr-coated nickel and Sn-coated steel samples were analyzed and the results agreed well with the results obtained by a glow discharge-OES method.

Material identification. Reliable identification of unknown materials is another interesting application of LIBS. Different statistical methods can be applied to sort materials according to their spectral signatures as each material is characterized by its unique LIBS spectrum.

Hybl[138] developed a method for accurate characterization of biological aerosols. Based on the fact that biological organisms contain a wide variety of inorganic elements such as Ca, Mg, Mn, Fe, P, Na, K and Si, LIBS, the elemental analysis technique, was incorporated in the biological sensor. The sensor used a 266-nm pulsed microchip laser to stimulate fluorescence from single biological particles. The fluorescence signal triggered a 50 mJ Nd:YAG laser to fire at individual particles. The high resolution LIBS spectra from individual particles were used in conjunction with principal component analysis to illustrate the ability of LIBS to distinguish different classes of bioaerosols using the ratios of atomic line intensities.

Our group has developed and successfully applied the LIBS-based method for identification of different classes of materials.[139–142] The method includes obtaining spectral data

from different substances and storing them in the form of a spectral library. Analysis of the unknown material is realized by correlating its spectrum against all spectra in the library and finding the closest match (Fig. 24). Parametric (linear) and non-parametric (rank) correlation methods were applied for identification of steel and cast iron samples,[139] particles,[140] plastics[141] and archeological artifacts.[142]

Biomedical. Analysis of biological substances by LIBS is challenging due to the specificity of bio-matrices. The specificity includes softness and destructiveness, high degree of inhomogeneity and low levels of concentrations of target elements. Nevertheless, the number of publications on LIBS in biomedical studies steadily increases.

Samek *et al.*[143] used LIBS for quantitative analysis of calcified tissue samples including teeth and bones. Information about spatial (lateral and depth) distribution of elements in teeth and bones was obtained upon continuous tracking/analyzing of ablation spectra. It was possible to link the quantitative results from LIBS analysis to environmental influences (*in vitro* studies of tooth or bone sample cross sections) and dental disease states (*in vivo* monitoring). A set of $CaCO_3$ pellets doped with target elements (Al, Sr, Pb) was used as reference samples in the range 100–10 000 ppm.

Telle[144] applied LIBS for screening of blood for traces of Rb. This could be a potential technique to trace the effect of illegal doping drugs. If rubidium chloride were given to an athlete around 30 min before competing and a sample of their blood (a drop on a filter) was subsequently tested for Rb content, the test would give a direct indication of the red blood cell count. In the experiment, rubidium nitride was used and trace levels down to 0.3% were successfully detected.

Forensic and military. LIBS seems to be an attractive technique for forensic and military applications as it offers fast *in situ* analysis at remote locations with satisfactory sensitivity in the part-per-million range.

A few forensic applications have recently been reported. Goode[145] analyzed gunshot residues taken from the shooter's hand after firing a weapon. Characteristic emission lines were observed from elements known to be present in gunshot residues, principally Ba and Pb. The sensitivity appeared to be excellent: even after washing the shooter's hands, detectable amounts of gunpowder remained.

Harmon[146] obtained LIBS spectra of explosive materials in a wide spectral range of 200–900 nm. These characteristic spectra could be readily identified in explosive residues on snow and in soil. This work suggested that there was the potential to develop a field-portable LIBS instrument for explosive detection, the standoff determination of buried landmines, and unexploded ordnance.

Art and archeology. There are several examples of application of LIBS for *in situ* analysis of precious artworks. Many of these applications utilize the fact that the technique is minimally destructive.

Anglos *et al.*[147] examined an 18th century oil painting subjected to partial restoration. Careful qualitative analysis of LIBS spectra obtained in a wide spectral range was performed. The different pigments used in the original and in the restored

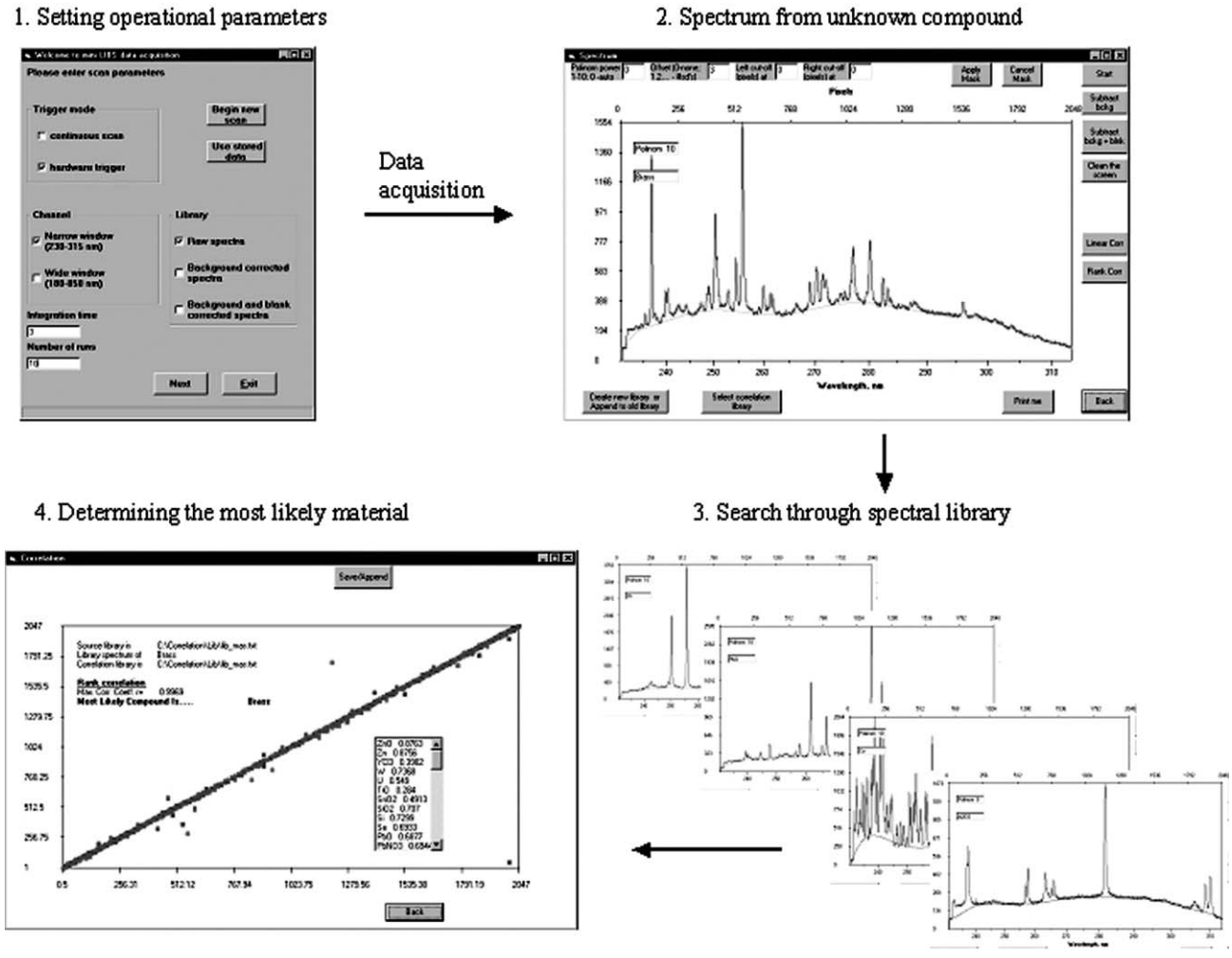

Fig. 24 Flow chart of the material identification methodology based on correlation analysis. References 139–142.

part of the work were clearly identified and precisely dated. The same method was later applied for precise dating of ancient manuscripts.[148] Cristoforetti *et al.*[149] used the micro-LIBS and micro-Raman techniques to analyze ancient pottery. Devos *et al.*[150] used LA-ICP-MS for authentication of antique silver objects. A special cell was designed to be placed upon the entire object for removing a microscopic amount of the sample and transporting it into the ICP-MS. The analytes Zn, Cd, Sn, Sb, Au, Pb and Bi were measured as indicators of the age of the objects. The method was shown to be sufficiently precise and accurate to allow "before/after" (1850) dating of antique silverware. The main advantage over wet techniques was virtual non-destructiveness and analysis speed.

Concluding remarks on LIBS

LIBS-based techniques have become increasingly popular in many applied fields. Operational simplicity, versatility and relatively low cost are the features which make LIBS the technique of choice for many research and industrial laboratories. Several commercial LIBS instruments have recently appeared on the market but the technology is still far from mass production and the cost of the commercial units is prohibitive for many low budget institutions. Certain anticipations can be linked to newly developed microchip lasers. The combination of microchip lasers with miniature spectral detectors can accelerate the mass production and convert LIBS into routine instrumentation in the nearest future, at least for applications which require portability and only moderate sensitivity.

The number of publications on both applications and fundamentals of laser ablation continued growing during the past several years. Among other positive achievements, extensive plasma modeling and deep understanding of processes involved in laser breakdown at all stages of light-material interaction should be particularly emphasized.

Overall conclusions

This paper has presented a personal view of the analytical performance of several spectroscopic techniques and shown the superiority of the "superstars", namely ETA-AAS, ICP-AES and ICP-MS, based upon the application of several selected figures of merit. Within the intrinsic limitation of the validity of such a comparison, the conclusions reached seem to be logical.

Some additional conclusive remarks seem to be in order, as follows.

(i) Some of the techniques compared to the super stars (*e.g.*, laser induced fluorescence and ionization) have a long history and an analytical tradition compared to other techniques recently developed (*e.g.*, cavity ringdown spectroscopy) or new techniques yet to be explored analytically (*e.g.*, NICE-OHMS).

(ii) As one of the first groups to develop laser excited fluorescence for the analysis of atoms and molecules, we would like to stress that atomic fluorescence and ionization spectroscopies will remain in an analytical niche, where high detection power and spectral selectivity are needed. As reported previously[26] these techniques still suffer from the common disadvantage that the general trend in analytical laser spectroscopy is still more focused on the development and optimization of a *single technique* rather than on combining more techniques in a *single instrument*.

(iii) Techniques such as RIS and RIMS can hardly be surpassed by any other technique in those case where isotopic selectivity and detection power are at stake: in these cases, the analyst has no choice left other than the use of these techniques, irrespective of how complex they are.

(iv) Absorption methodologies based on cavity-enhanced detection will definitely continue to thrive. As a consequence, our current comparison will definitely need to be updated in the near future.

(v) Despite the current, well-deserved, interest of the analytical spectroscopic community, it is only fair to say that LIBS is not the cure for all analytical problems involving rapid, *in-situ*, qualitative and quantitative elemental and molecular analysis of all species of environmental, industrial, forensic and biological importance.

(vi) Finally, it is tempting to ask whether one should give up research and applications on atomic spectroscopy methods other than the three superstars. The answer is a *strong no*. We hope that this review has served the purpose of highlighting several new exciting avenues and approaches to the continuous development of analytical methodologies with lasers. Their success and acceptance will largely depend upon an increase in the number of laboratories involved with these methods.

Acknowledgements

This work was supported by DOE-DE-FG02-99ER14960.

References

1 H. A. Laitinen, *Anal. Chem.*, 1973, **44**, 2305.
2 V. A. Fassel, *Z. Anal. Chem.*, 1986, **324**, 511.
3 G. M. Hieftje, *Spectrochim. Acta (Vatican Issue)*, 1989, **44B**, 113.
4 G. M. Hieftje, *J. Chem. Educ.*, 2000, **77**, 579.
5 *Spectroscopy*, "The Application Notebook", February, 2003, p. 41.
6 J. D. Winefordner, I. B. Gornushkin, D. Pappas, O. I. Matveev and B. W. Smith, *J. Anal. At. Spectrom.*, 2000, **15**, 1161.
7 G. M. Hieftje, *J. Anal. At. Spectrom.*, 1996, **11**, 613.
8 *Inductively Coupled Plasma Mass Spectrometry*, ed. A. Montaser, John Wiley, New York, 1998.
9 J. S. Becker and H.-J. Dietze, *Spectrochim. Acta*, 1998, **53B**, 1475.
10 R. S. Houk, *Accounts Chem. Res.*, 1994, **27**, 333.
11 J. A. C. Broekaert, *Analytical Atomic Spectrometry with Flames and Plasmas*, Wiley-VCH, Weinheim, 2001.
12 B. Welz and M. Sperling, *Atomic Absorption Spectrometry*, Wiley-VCH, New York, 3rd edn., 1999.
13 K. W. Busch and M. A. Busch, *Cavity Ringdown Spectroscopy*, ACS Symposium Series 720, American Chemical Society, Washington, DC, 1999.
14 A. T. Ince, J. B. Dawson and J. Snook, *J. Anal. At. Spectrom.*, 1996, **11**, 967.
15 A. Miklos, *Anal. Chem.*, 2000, **30A**, 1.
16 X. Yao, S. P. McGlynn and R. C. Mohanty, *Microchem. J.*, 1999, **61**, 223.
17 X. Hou, P. Stchur, K. X. Yang and R. G. Michel, *Trends Anal. Chem.*, 1999, **17**, 532.
18 P. Stchur, K. X. Yang, X. Hou, T. Sun and R. G. Michel, *Spectrochim. Acta*, 2001, **56B**, 1565.
19 *Analytical Laser Spectroscopy*, ed. N. Omenetto, Wiley-Interscience, New York, 1979, vol. 50.
20 *Analytical Applications of Lasers*, ed. E. H. Piepmeier, Wiley-Interscience, New York, 1986, vol. 87.
21 J. C. Travis and G. C. Turk, *Laser Enhanced Ionization Spectrometry*, Wiley-Interscience, New York, 1996, vol. 136.
22 V. S. Letokhov, *Laser Photoionization Spectroscopy*, Academic Press, Orlando, FL, 1987.
23 *Applied Laser Spectroscopy: Techniques, Instrumentation, and Applications*, ed. D. L. Andrews, VCH, New York, 1992.
24 G. S. Hurst and M. G. Payne, *Principles and Applications of Resonance Ionization Spectroscopy*, IOP Publishing, Adam Hilger, Bristol, 1988.
25 B. A. Bushaw, W. Norterhäuser and K. Wendt, *Spectrochim. Acta*, 1999, **54B**, 321.
26 N. Omenetto, *J. Anal. At. Spectrom.*, 1998, **13**, 385.
27 H. Kaiser, *Spectrochim Acta*, 1978, **33B**, 551.
28 H. Kaiser, *Two Papers on the Limit of Detection of a Complete Analytical Procedure*, Hafner, New York, 1969.
29 H. Kaiser, *Anal. Chem.*, 1970, **42**(2), 24A.
30 H. Kaiser, *Anal. Chem.*, 1970, **42**(4), 26A.
31 IUPAC, Analytical Chemistry Division, *Spectrochim. Acta*, 1978, **33B**, 242.
32 K. Fujiwara, J. A. McHard, S. J. Foulk, S. Bayer and J. D. Winefordner, *Can. J. Spectrosc.*, 1980, **25**, 18.

33 J. D. Winefordner, G. A. Petrucci, C. L. Stevenson and B. W. Smith, *J. Anal. At. Spectrom.*, 1994, **9**, 131.
34 C. Th. J. Alkemade, *Appl. Spectrosc.*, 1981, **35**, 1.
35 C. L. Stevenson and J. D. Winefordner, *Chemtracts-Anal., Phys. Inorg. Chem.*, 1990, **2**, 217.
36 C. L. Stevenson and J. D. Winefordner, *Appl. Spectrosc.*, 1992, **46**, 407.
37 H. Falk, *J. Anal. At. Spectrom.*, 1992, **7**, 255.
38 J. D. Winefordner, B. W. Smith and N. Omenetto, *Spectrochim. Acta*, 1989, **44B**, 1397.
39 P. Hannaford, *Spectrochim. Acta*, 1999, **54B**, 2183.
40 O. Axner, Talk at XXXIII CSI in Granada, Spain, Sept. 9, 2003.
41 P. Kluczynski, J. Gustafson, A. M. Lindberg and O. Axner, *Spectrochim. Acta*, 2001, **56B**, 1277.
42 H. Groll and K. Niemax, *Spectrochim. Acta*, 1993, **48B**, 633.
43 A. Zybin, C. Schnürer-Patschan, M. A. Bolshov and K. Niemax, *Trends Anal. Chem.*, 1998, **17**, 513.
44 P. Kluczynski, A. M. Lindberg and O. Axner, *Appl. Opt.*, 2000, **40**, 783.
45 P. Kluczynski, A. M. Lindberg and O. Axner, *Appl. Opt.*, 2001, **40**, 794.
46 J. Ye, L. S. Ma and J. Hall, *J. Opt. Soc. Am.*, 1998, **15**, 6.
47 J. Ye, P. Dube and J. Hall, *J. Opt. Soc. Am.*, 1999, **16**, 225 5b.
48 S. L. Mandelstam and V. V. Nedler, *Spectrochim. Acta*, 1961, **17**, 885.
49 A. Walsh, *Spectrochim. Acta*, 1955, **7**, 108.
50 B. V. L'Vov, *Spectrochim. Acta*, 1961, **17**, 761.
51 L. De Galan, *Anal. Chim. Acta*, 1966, **34**, 2.
52 L. De Galan, *Particle Distribution in the D.C. Carbon Arc*, PhD Dissertation, University of Amsterdam, 1965.
53 P. W. J. M. Boumans, *Theory of Spectrochemical Excitation*, Plenum Press, New York, 1966.
54 C. S. Rann, *Spectrochim. Acta*, 1968, **23B**, 827.
55 L. De Galan and G. F. Samaey, *Anal. Chim. Acta*, 1970, **50**, 391.
56 B. V. L'Vov, *Spectrochim. Acta*, 1978, **33B**, 153.
57 B. V. L'Vov, V. G. Nikolaev, E. A. Norman, L. K. Polzik and M. Mojica, *Spectrochim. Acta*, 1986, **41B**, 1043.
58 B. V. L'Vov, *J. Anal. At. Spectrom.*, 1988, **3**, 9.
59 D. Bulajic, M. Corsi, G. Cristoforetti, S. Legnaioli, V. Palleschi, A. Salvetti and E. Tognoni, *Spectrochim. Acta*, 2002, **57B**, 339.
60 U. Gorlach and C. F. Boutron, in *Heavy Metals in the Environment*, ed. J. P. Vernet, CEP Consultants, Edinburgh, U.K., 1989.
61 E. W. Wolff, *Antarctic Sci.*, 1990, **2**, 189.
62 C. F. Boutron, J. P. Candelone and S. Hong, *Geochim. Cosmochim. Acta*, 1994, **58**, 3217.
63 P. R. Trincherini, in *Alfred O. Nier Symposium on Inorganic Mass Spectrometry*, Durango, Colorado, USA, 1994.
64 P. R. Trincherini, F. Mousty, R. Passarella, V. Pedroni and A. Poletteris, *J. Trace Microprobe Technol.*, 1993, **10**, 295.
65 V. A. Korneev, V. K. Ivanov, A. M. Pchelinstev, J. F. Odinochkina and V. A. Agratemin, *J. Appl. Spectrosc. (USSR)*, 1990, **52**, 335.
66 H. J. Graf and W. L. Reynolds, *Solid State Technical*, 1985, 141.
67 R. Van Grieken and C. Xhoffer, *J. Anal. At. Spectrom.*, 1992, **7**, 81.
68 K. A. Prather, T. Nordmeyer and K. Salt, *Anal. Chem.*, 1994, **66**, 1403.
69 K. P. Hinz, R. Kaufmann and B. Spengler, *Anal. Chem.*, 1994, **66**, 2071.
70 J. M. Dale, M. Yang, W. B. Whitten and J. M. Ramsey, *Anal. Chem.*, 1994, **66**, 3431.
71 T. Nordmeyer and K. A. Prather, *Anal. Chem.*, 1994, **66**, 3540.
72 B. A. Mansoori, M. V. Johnston and A. S. Wexler, *Anal. Chem.*, 1994, **66**, 3681.
73 L. J. Radziemski, *Spectrochim. Acta*, 2002, **57B**, 1109.
74 L. J. Radziemski and P. A. Cremers, *Laser Induced Plasmas and Applications*, Marcel Dekker, New York, 1989.
75 T. H. Maiman, *Nature*, 1960, **187**, 493–494.
76 F. Brech and L. Cross, *Appl. Spectrosc.*, 1962, **16**, 59.
77 E. R. Runge, R. W. Minck and F. R. Bryan, *Spectrochim. Acta*, 1964, **20**, 733.
78 N. G. Basov and O. N. Krokhin, *Sov. Phys. JETP*, 1964, **19**, 123.
79 Y. B. Zel'dovich and Y. P. Raizer, *Sov. Phys. JETP*, 1965, **20**, 772.
80 J. F. Ready, *Effects of High-Power Laser Radiation*, Academic Press, New York, 1971.
81 C. Aragon, V. Madurga and J. A. Aguilera, *Appl. Surf. Sci.*, 2002, **197–198**, 217–223.
82 V. M. Villagran-Muniz, H. Sobral, R. Navarro-Gonzalez, P. F. Velazquez and A. C. Raga, *Plasma Physics and Controlled Fusion*, 2003, **45**, 571–584.
83 P. K. Kennedy, *IEEE J. Quant. Electronics*, 1995, **31**, 2241–2249.
84 R. F. Haglund, Jr., "Mechanisms of Laser-Induced Desorption and Ablation", in *Laser Ablation and Desorption*, ed. J. C. Miller and R. F. Haglund, Jr., Experimental Methods in Physical Sciences, Academic Press, 1998.
85 G. M. Weyl, "Physics of Laser-Induced Breakdown: An Update", in *Laser-Induced Plasmas and Applications*, ed. L. J. Radziemski and D. A. Cremers, Marcel Dekker, Inc., New York, 1989.
86 C. A. Sacchi, *J. Opt. Soc. Am. B*, 1991, **8**, 337–345.
87 D. Kim, M. Ye and C. P. Grigoropoulos, *Appl. Phys. A*, 1998, **67**, 169–181.
88 M. D. Perry, B. C. Stuart, P. S. Banks, M. D. Feit, V. Yanovsky and A. M. Rubenchik, *J. Appl. Phys.*, 1999, **85**, 6803–6810.
89 X. Mao, S. S. Mao and R. E. Russo, *Appl. Phys. Lett.*, 2003, **82**, 697–699.
90 J. G. Lunney and R. Jordan, *Appl. Surf. Sci.*, 1998, **127–129**, 941–946.
91 G. Callies, H. Schittenhelm, P. Berger and H. Hügel, *Appl. Surf. Sci.*, 1998, **127–129**, 134–141.
92 S. Yalçin, D. R. Crosley, G. P. Smith and G. W. Faris, *Appl. Phys. B*, 1999, **68**, 121–130.
93 J. Hermann, C. Boulmer-Leborgne and D. Hong, *J. Appl. Phys.*, 1998, **83**, 691–696.
94 A. Casavola, G. Colonna and M. Capitelli, *Appl. Surf. Sci.*, 2003, **208–209**, 85–89.
95 G. Colonna, A. Casavola and M. Capitelli, *Spectrochim. Acta, Part B*, 2001, **56**, 567–586.
96 T. E. Itina, J. Hermann, Ph. Delaporte and M. Sentis, *Appl. Surf. Sci.*, 2003, **208–209**, 27–32.
97 J. R. Ho, C. P. Grigoropoulos and J. A. C. Humphrey, *J. Appl. Phys.*, 1996, **79**, 7205–7215.
98 V. I. Mazhukin, V. V. Nossov, M. G. Nickiforov and I. Smurov, *J. Appl. Phys.*, 2003, **93**, 56–66.
99 V. I. Mazhukin, V. V. Nossov and I. Smurov, *J. Appl. Phys.*, 2001, **90**, 607–618.
100 V. I. Mazhukin, V. V. Nossov, G. Flamant and I. Smurov, *J. Quant. Spectr. Radiat. Transfer*, 2002, **73**, 451–460.
101 I. B. Gornushkin, C. L. Stevenson, B. W. Smith, N. Omenetto and J. D. Winefordner, *Spectrochim. Acta, Part B*, 2001, **56**, 1769–1785.
102 I. B. Gornushkin, A. Ya. Kazakov, N. Omenetto, B. W. Smith and J. D. Winefordner, *Spectrochim. Acta, Part B*, 2004, in the press.
103 A. Ciucci, M. Corsi, V. Palleschi, S. Rastelli, A. Salvetti and E. Tognoni, *Appl. Spectrosc.*, 1999, **53**, 960–964.
104 D. Bilajic, M. Corsi, G. Cristoforetti, S. Legnaioli, V. Palleschi, A. Salvetti and E. Tognoni, *Spectrochim. Acta, Part B*, 2002, **57**, 339–353.
105 L. M. Cabalin and J. J. Laserna, *Spectrochim. Acta, Part B*, 1998, **53**, 723–730.
106 G. W. Rieger, M. Taschuk, Y. Y. Tsui and R. Fedosejevs, *Spectrochim. Acta, Part B*, 2003, **58**, 497.
107 R. E. Russo, *Appl. Spectrosc.*, 1995, **49**, 14A–28A.
108 W. T. Chan and R. E. Russo, *Spectrochim. Acta, Part B*, 1991, **46**, 1471–1486.
109 J. Gonzalez, X. L. Mao, J. Roy, S. S. Mao and R. E. Russo, *J. Anal. At. Spectrom.*, 2002, **17**, 1108–1113.
110 M. Motelica-Heino, P. Le Coustumer and O. F. X. Donard, *J. Anal. At. Spectrom.*, 2001, **16**, 542–550.
111 B. N. Chichkov, C. Momma, S. Nolte, F. von Alvensleben and A. Tunnermann, *Appl. Phys.*, 1996, **63**, 109–115.
112 B. Sallé, O. Gobert, P. Meynadier, M. Perdrix, G. Petite and A. Semerok, *Appl. Phys. A [Suppl.]*, 1999, **69**, S381–S383.
113 M. D. Perry, B. C. Stuart, P. S. Banks, M. D. Feit, V. Yanovsky and A. M. Rubenchik, *J. Appl. Phys.*, 1999, **85**, 6803–6810.
114 M. Lenzner, J. Krüger, S. Sartania, Z. Cheng, Ch. Spielmann, G. Mourou, W. Kautek and F. Krausz, *Phys. Rev. Lett.*, 1998, **80**, 4076–4079.
115 E. Tognoni, V. Palleschi, M. Corsi and G. Cristoforetti, *Spectrochim. Acta, Part B*, 2002, **57**, 1115–1130.
116 L. St.-Onge, M. Sabsabi and P. Cielo, *Spectrochim. Acta, Part B*, 1998, **53**, 407–415.
117 D. N. Stratis, K. L. Eland and S. M. Angel, *Appl. Spectrosc.*, 2000, **54**, 1270–1274.
118 M. Lapczyna, K. P. Chen, P. R. Herman, H. W. Tan and R. S. Marjoribanks, *Appl. Phys. A [Suppl.]*, 1999, **69**, S883–S886.
119 J. J. Zayhowski, *J. Alloys Compd*, 2000, **303–304**, 393–400.

120 I. B. Gornushkin, B. W. Smith, N. Omenetto and J. D. Winefordner, *Appl. Spectrosc.*, submitted for publication.
121 S. Eppler, A. Cremers, D. Hickmott, J. Ferris and C. Koskelo, *Appl. Spectrosc.*, 1996, **50**, 1175.
122 C. Chaléard, P. Mauchien, N. Andre, J. Uebbing, J. L. Lacour and C. J. Geertsen, *J. Anal. At. Spectrom.*, 1997, **12**, 183–188.
123 S. I. Gornushkin, I. B. Gornushkin, J. M. Anzano, B. W. Smith and J. D. Winefordner, *Appl. Spectrosc.*, 2002, **56**, 433–436.
124 S. Shuttleworth and D. T. Kremser, *J. Anal. At. Spectrom.*, 1998, **13**, 697–700.
125 L. M. Berman and P. J. Wolf, *Appl. Spectrosc.*, 1998, **52**, 438–443.
126 P. Fichet, P. Mauchien, J.-F. Wagner and C. Moulin, *Anal. Chim. Acta*, 2001, **429**, 269–278.
127 J. Noak, D. X. Hammer, G. D. Noojin, B. A. Rockwell and A. Vogel, *J. Appl. Phys.*, 1998, **83**, 7488.
128 A. Vogel, J. Noack, K. Nahen, D. Theisen, S. Busch, U. Parlitz, D. X. Hammer, G. D. Noojin, B. A. Rockwell and R. Birngruber, *Appl. Phys. B*, 1999, **68**, 271.
129 A. Kuwako, Y. Uchida and K. Maeda, *Proceedings Laser Induced Plasma Spectroscopy and Applications*, Orlando, Fl., 2002, pp. 109–111.
130 L. Dudragne, Ph. Adam and J. Amouroux, *Appl. Spectrosc.*, 1998, **52**, 1321–1327.
131 H. Zhang, F.-Y. Yueh and J. P. Singh, *Appl. Opt.*, 1999, **38**, 1459–1466.
132 D. Hahn, *Appl. Phys. Lett.*, 1998, **72**, 2960–2962.
133 D. W. Hahn, W. L. Flower and K. R. Hencken, *Appl. Spectrosc.*, 1997, **51**, 1836–1844.
134 B. W. Smith, D. W. Hahn, E. Gibb, I. Gornushkin and J. D. Winefordner, *KONA*, 2001, **19**, 25–32.
135 J. E. Carranza, B. T. Fisher, G. D. Yoder and D. W. Hahn, *Spectrochim. Acta, Part B*, 2001, **56**, 851–864.
136 V. Margetic, M. Bolshov, A. Stokhaus, K. Niemax and R. Hergenröder, *J. Anal. At. Spectrom.*, 2001, **16**, 616–621.
137 C. C. García, M. Corral, J. M. Vadillo and J. J. Laserna, *Appl. Spectrosc.*, 2000, **54**, 1027–1031.
138 J. D. Hybl, G. A. Lithgow and S. G. Backley, *Appl. Spectrosc.*, 2003, **37**, 1207.
139 I. B. Gornushkin, B. W. Smith, H. Nasajpour and J. D. Winefordner, *Anal. Chem.*, 1999, **71**, 5157–5164.
140 I. B. Gornushkin, A. Ruiz-Medina, J. M. Anzano, B. W. Smith and J. D. Winefordner, *J. Anal. At. Spectrom.*, 2000, **15**, 581–586.
141 J. M. Anzano, I. B. Gornushkin, B. W. Smith and J. D. Winefordner, *J. Polymer Sci. Technol.*, 2000, **40**, 2423–2429.
142 J. M. Anzano, M. A. Villoria, I. B. Gornushkin, B. W. Smith and J. D. Winefordner, *Can. J. Anal. Sci. Spectrosc.*, 2002, **47**, 134–140.
143 O. Samek, D. S. C. Beddows, H. H. Telle, J. Kaiser, M. Liška, J. O. Cáseres and A. Gonzáles Ureña, *Spectrochim. Acta, Part B*, 2001, **56**, 865–875.
144 M. O. Al-Jeffery and H. Telle, *Proceedings of SPIE—The International Society for Optical Engineering*, Optical Biopsy IV, San Jose, CA, vol. 4613, 2002, pp. 152–161.
145 S. R. Goode, C. R. Dockery, M. F. Bachmeyer, A. A. Nieuwland and S. L. Morgan, *Proceedings Laser Induced Plasma Spectroscopy and Applications*, Orlando, FL, 2002, pp. 175–177.
146 R. S. Harmon, A. W. Miziolek, K. L. McNesby, T. F. Jenkins and M. Walsh, *Proceedings Laser Induced Plasma Spectroscopy and Applications*, Orlando, Fl, 2002, pp. 184–185.
147 D. Anglos, S. Couris and C. Fotakis, *Appl. Spectrosc.*, 1997, **51**, 1025–1030.
148 K. Melessanaki, V. Papadakis, C. Balas and D. Anglos, *Spectrochim. Acta, Part B*, 2001, **56**, 2337–2346.
149 G. Cristoforetti, M. Corsi, M. Giuffrida, M. Hidalgo, D. Iriarte, S. Legnaioli, V. Palleschi, A. Salvetti, E. Tognoni, G. Boschian and S. Mazzoni, *Proceedings. Laser Induced Plasma Spectroscopy and Applications*, Orlando, Fl, 2002, pp. 209–211.
150 W. Devos, C. Moor and P. Lienemann, *J. Anal. At. Spectrom.*, 1999, **14**, 621–626.